Nanoscale

Accepted Manuscript

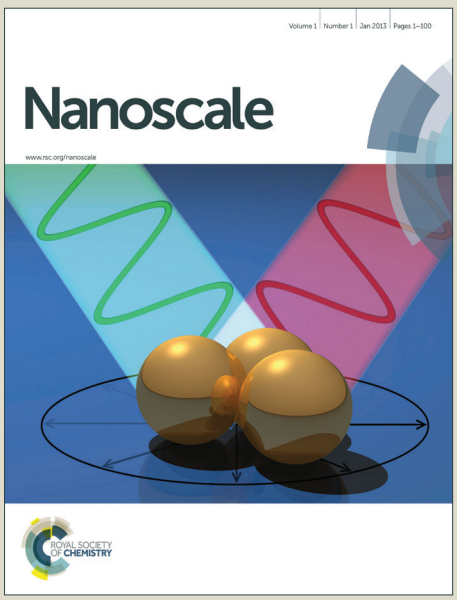

ROYAL SOCIETY OF CHEMISTRY

www.rsc.org/nanoscale

Nanohybrid Conjugated Polyelectrolytes: Highly Photostable and Ultrabright Nanoparticles

*Ghinwa H. Darwish, Pierre Karam**

Department of Chemistry, American University of Beirut, P.O. Box 11-0236, Beirut, Lebanon

KEYWORDS: Conjugated polyelectrolytes, Photostability, Fluorescent enhancement, MPS-PPV, polyvinylpyrrolidone , Single Molecule Spectroscopy.

We present a general and straightforward one-step approach to enhance the photophysical properties of conjugated polyelectrolytes. Upon complexation with an amphiphilic polymer (polyvinylpyrrolidone), an anionic conjugated polyelectrolyte (Poly[5-methoxy-2-(3-sulfopropoxy)-1,4phenylenevinylene]) was prepared into small nanoparticle with exceptional photostability and brightness. The polymer fluorescence intensity was enhanced by 23 folds and could be easily tuned by changing the order of addition. Single molecule experiments revealed a complete suppression of blinking. In addition, after only losing 18% of the original intensity, a remarkable amount of photons were emitted per particle (~10^9, on average). This number is many folds greater than popular organic fluorescent dyes. We believe an intimate contact between the two polymers is shielding the conjugated polyelectrolyte from the destructive photooxidation. The prepared nanohybrid particles will prove instrumental in single particle based fluorescent assays and can serve as a probe for current state-of-the-art bioimaging fluorescent techniques.

Conjugated polyelectrolytes (CPEs) are remarkable materials with enormous range of applications.[1, 2] They have been implemented in cheap organic solar cells,[3-5] and as new promising class of antibacterial agents[6] and were recently used as efficient fusiogenic materials.[7] They were particularly useful in developing single particle based bio- and chemical sensing assays.[1, 8-12] CPEs can detect the presence of fluorescent quenchers with exquisite and amplified sensing capabilities.[13-16] As such, they were successfully used to sense specific oligonucleotides sequences,[11, 17-19] small molecules,[20] biomolecules[21] and discriminate between different bacteria strains.[22] Given their low cytotoxicity, compared to quantum dots, numerous attempts were geared towards developing them into targeted fluorescent probes for cell imaging applications.[23, 24]

Despite their huge potentials, they still suffer from blinking, fast irreversible photobleaching and low quantum yield efficiency. This has therefore limited their wide spread implementation into long shelf life sensing devices and probes for bioimaging and single particle tracking applications. Such techniques require exceptional photostability and brightness to obtain significant spatial and temporal information on the target or the cellular and subcellular structures they probe. It took laborious ensemble and single-molecule spectroscopy studies to understand and improve CPEs photophysical properties.[14, 25, 26]

CPEs backbones are prone to chemical oxidation by singlet oxygen leading to the creation of a permanent photochemical defects that quenches their excitations.[27] Their fluorescence emission originates from individual chromophores presumably delimited by twists that breaks the π–π orbitals delocalization and creates multiple emissive sites.[28] As such, polymer photophysics strongly correlates with its backbone conformation and its solvated state.[25] It dictates the energy transfer efficiency between neighboring chromophores. For instance, in water, conjugated

polyelectrolytes adopt a highly coiled conformation to minimize the interaction between its hydrophobic backbone and the nonpolar solvent. The collapsed state induces stresses along the backbone leading to the formation of kinks and defective sites, which can serve as trapping and nonradiative recombination sites. The aggregated state also results in the formation of shorter chromophores and long range ordered and highly packed chains thus favoring efficient interchain or through-space energy transfer, which strongly compete with radiative emission processes.[24] The combined effects result in low quantum yield and overall mediocre photophysical properties in water as compared to other nonpolar solvents. Specifically, recent single molecule studies demonstrated this direct correlation between the CPE conformation/solvation state and its spectroscopic properties.[26] When anionic conjugated polyelectrolyte, poly[5-methoxy-2-(3-sulfopropoxy)-1,4-phenylene-vinylene] (MPS-PPV), is encapsulated in negatively charged liposomes, it exists in a freely diffusing yet as a collapsed state. Discrete fluorescence intensity levels and individual on-off transition steps were reported in the single-particle fluorescence intensity-time trajectories. This quantized behavior reflects the efficient interchain exciton transport to localized fluorescence quenching sites along the PPV backbone (oxidation, kinks etc). In marked contrast, extended polymer chains embedded within the lipid membranes showed exponential decrease in intensity over time. This behavior is characteristic of the photobleaching of a collection of multiple independent chromophores. When compared to the aggregated/collapsed structure, the relatively extended CPEs showed brighter intensities and better photostability.

Building on the knowledge gained from steady state fluorescent experiments and single molecule studies, polyelectrolytes and surfactants were used to facilitate CPEs solubility and favor backbone disaggregation. [7, 29, 30] In return, these structures provided enhanced fluorescence

performance with excellent sensing capabilities down to the single molecule level.[9, 31, 32] Other approaches employed metal enhanced fluorescence methods to increase the CPE quantum yield from, for instance, 3 to 77% by positioning a polythiophene conjugated polymer close to a spherical silver nanoparticle separated by a silica spacer.[33]

The presence of specific surfactants and metallic nanoparticles, however, limited the application of CPEs. New strategies to disaggregate the polymer have emerged by deliberately engineering the polymer side chains and its backbone.[34] PPE-based conjugated polyelectrolytes were modified with dendritic poly(benzyl ether) terminated with carboxylic acid groups as side chains.[35] With each dendrimer generation, the backbone charge density increased, resulting in its disaggregation and subsequent increase in its fluorescence quantum yield. Recently, a more surgical approach was reported; the oxygen atom directly connected to the phenylene rings in a PPE-based CPE was substituted with a carbon atom.[36] This modification suppressed the tendency of the polymer to aggregate in water and the quantum yield increased from 4 to 16%. However, these modifications remain specific to a narrow class of conjugated polyelectrolytes.

CPEs also suffer from low photostability due to the destructive effect of singlet oxygen.[37] In some cases, the addition of surfactants shielded the conjugated backbone from oxygen. [38] Additives did also improve on the polymer photophysics. Liu *et al.* have reported on the healing effect of β-mercaptoethanol (BME), a known antioxidant, on photooxidated CPE.[39] Although BME was able to recover the fluorescence loss of CPEs for multiple cycles, it did not prevent the photodegradation of CPEs.

Consequently, there exists a major challenge to improve CPEs fluorescent efficiency and photostability while increasing their functionality. Previous attempts introduced stringent

conditions that often narrowed the CPE spectrum of applications. In this work, we report a straightforward and a general approach to increase the fluorescence quantum yield and, most importantly, enhance the photostability of a commercially available conjugated polyelectrolyte MPS-PPV. Polyvinylpyrrolidone (PVP), an amphiphilic polymer, was used as a scaffold to extend the polymer backbone and protect it from photodegradation which resulted in a 23 folds increase in its quantum efficiency. Single particle studies revealed the emission of a remarkable number of photons per particle. On average, 10^9 photons were emitted when the fluorescent signal was only 18% down from its initial intensity. All traces showed no sign of blinking during our experiment time window. The prepared hybrid particles were estimated to be in the range of few nm in diameters (*ca.* hydrodynamic 15-20nm). In this report, we will address fundamental questions such as how is PVP protecting the vulnerable CPE from photodegradation and how is it enhancing its photophysical properties? Our findings are significant, as they present a facile approach to prepare bright and highly photostable conjugated polyelectrolytes.

Results and Discussions:

Hybrid nanoparticle design: In this study, we used the anionic Poly[5-methoxy-2-(3-sulfopropoxy)-1,4phenylenevinylene] (MPS-PPV) (Figure 1A) as a surrogate/model system to investigate the effect of an amphiphilic macromolecule on improving the photophysical properties of CPEs. MPS-PPV is commercially available and has been extensively used as a platform for biosensing schemes. In addition, its photophysical properties have been studied at the ensemble and single molecule levels.[26, 30, 39]

Our strategy was to search for an amphiphilic macromolecule that would disaggregates the hydrophobic backbone of MPS-PPV through strong and stable complexation/interactions

contacts. Consequently, this will allow us to efficiently dissolve and extend the polymer backbone, and enhances its water solubility and photophysical properties. The macromolecule, in addition, should be readily modified to indirectly introduce chemical functionality to existing conjugated polyelectrolytes. To fulfill these purposes, we chose polyvinylpyrrolidone (PVP) (Figure 1B) which is considered a safe material and has been approved by FDA for many medical uses. PVP has been extensively used to prepare biocompatible nanoparticles, drug delivery vehicles and passivate biomaterial surfaces.[40, 41] It could be also prepared with a terminal primary amine or a carboxylic acid group.[42, 43] Specific biomolecules or small organic molecules of interest could be then introduced. This in turn adds an array of potential functionality and applications to the prepared hybrid structure while avoiding the complexity that accompanied the direct CPEs chemical modifications.

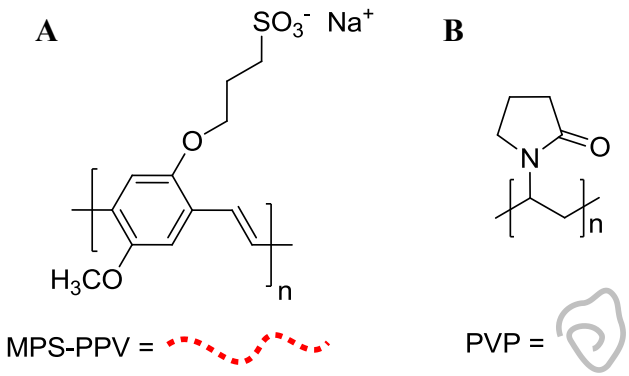

Figure 1: Chemical structures and their equivalent cartoon representations of (A) the anionic conjugated polyelectrolyte Poly[5-methoxy-2-(3-sulfopropoxy)-1,4phenylenevinylene] sodium (MPS-PPV) and (B) the amphiphilic macromolecule polyvinypyrolidone (PVP).

The hybrid particles were prepared by mixing a solution of MPS-PPV with different molecular weights of PVP. We characterized the particles by performing light scattering experiments. Particles size distribution (table 1, SI), revealed an average hydrodynamic diameter in the

nanosize range between 15nm - 20 nm. When compared to PVP alone, we observed an increase in the average diameter for each respective hybrid particle. Given their size, the prepared structure will be therefore referred to as "nanohybrid particle(s)". Of importance, the prepared particles were stable in solution for weeks without any signs of aggregation or precipitation.

Fluorescent Enhancement: To probe the interactions between the CPE and the amphiphilic polymer, we monitored the spectroscopic properties of MPS-PPV with and without PVP (55K). We followed the changes in MPS-PPV fluorescent emission when adding incremental amounts of the amphiphilic polymer. The enhancement was calculated as the ratio of the maximum emission intensity recorded after each addition of PVP to that of the pristine MPS-PPV (Figure 2 A). A 23-fold increase in fluorescent enhancement is observed followed by a plateau at approximately $5x10^{-5}$M in amphiphilic polymer concentration. The enhancement is ascribed to the deaggregation of the conjugated polymer backbone upon PVP complexation. As a result, the isolated chains inhibit efficient interchain coupling suppressing the possible self-quenching pathway. This strong interaction is presumably to be driven by a combination of hydrophobic contacts between the two polymer backbones, and by favorable entropy changes upon release of interfacial water molecules. The photoluminescence quantum yield of the hybrid structure was calculated to be equal to 23%. The brightness of the prepared hybrid structure was found to be equal to 420, which is significantly larger than most organic fluorescent dyes (typical reported values are <90).[44] Limited brightness of conventional dyes often results in low signal-to-background and is considered a major hurdle in sensing and single molecule fluorescence experiments.

Contrary to earlier reports, where a blue shift in the fluorescence emission was observed upon conjugated polyelectrolytes deaggregation, our results show a red shift (ca. 520 to 550 nm) thus

revealing a different interaction mechanism (Figure 2B). It was argued in previous reports that upon polymer backbone deaggregation exciton funneling to lower energy sites (red chromophores) and quenching sites can be dramatically inhibited. As such, fluorescence enhancement is often accompanied by a blue shift in the emission spectrum.

In our specific case, while the previous hypothesis still applies, it is reasonable to assume that the red shift is due to the increase in chromophore conjugation length, a phenomenon that is observed with increasing oligomer conjugation length.[45] We reasoned that upon PVP complexation, MPS-PPV chromophore length increases as a result of the suppression of the torsional motion. Interchain energy transfer to quenching sites, as expected, is also reduced. This will lead to the observed fluorescent enhancement and red-shift in the fluorescence emission spectra. In addition, the presence of PVP induced a 20 nm red shift in the CPE maximum absorbance concomitant with a slight increase in its absorbance (Figure 2C). This shift in absorbance confirms the formation of extended chromophores (i.e. red species).[45] Very recently, a report by Godin *et al.* described the fluorescent enhancement of MPS-PPV prepared in different solvent mixtures (H_2O/THF).[46] In low water content, nanoparticles (110-212 nm) exhibited a red-shift in the emission which was also attributed to the increase in conjugation length of MPS-PPV.

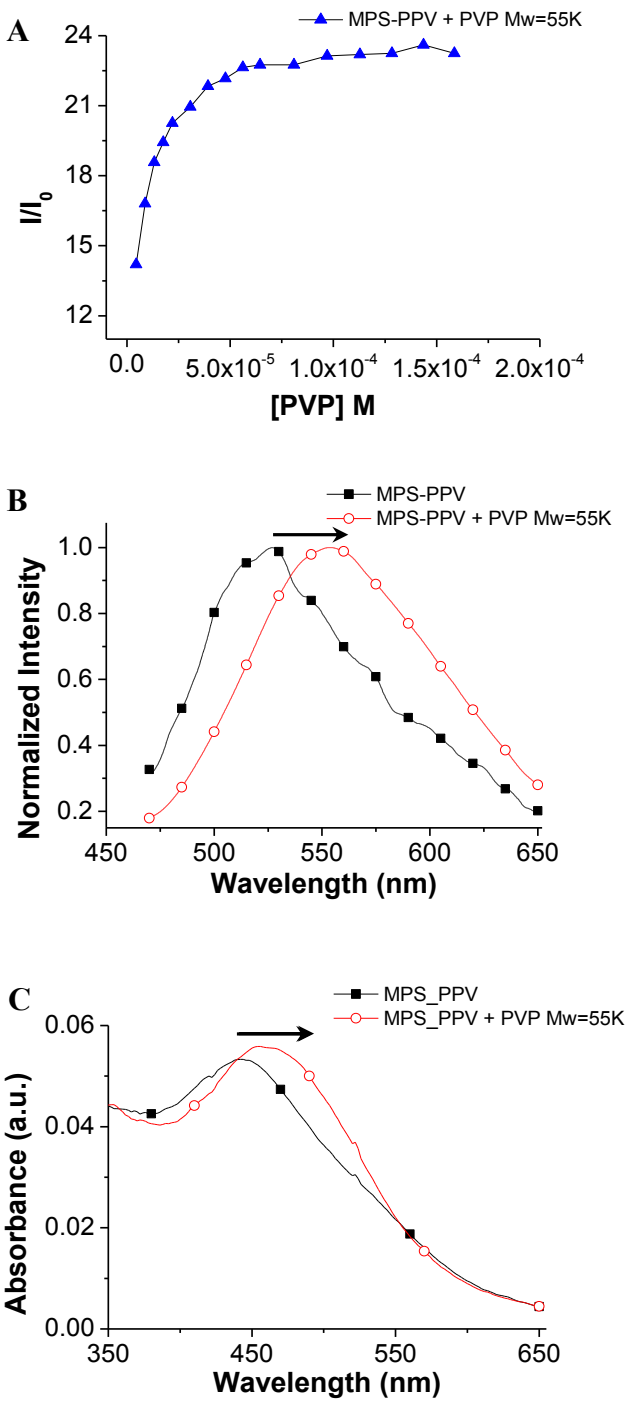

Figure 2: (A) Fluorescence emission enhancement of MPS-PPV ($1.6x10^{-4}$M in monomer concentration) upon addition of incremental amounts of PVP (MW=55K). The fluorescence ratio was calculated by dividing the maximum intensity after each addition to the maximum fluorescence emission of pristine MPS-PPV. The lines connecting the experimental points are for

visual aid. (B) Normalized fluorescence intensity and (C) absorbance spectra of pristine MPS-PPV and MPS-PPV_PVP. The polymer concentrations are: MPS-PPV=$1.6x10^{-4}$M (reported in monomer concentration) and PVP =$5x10^{-5}$M (reported in polymer concentration). All measurements were done in 10 mM HEPES buffer pH=7.3 and 150 mM NaCl and emission spectra were acquired upon excitation at 450nm.

Polymer-Polymer interaction: To gain an insight on the PVP/CPE interaction, we examined the effect of PVP molecular weight on the fluorescence enhancement. Four different molecular weights were tested and compared 10K, 55K, 360K and 1300K (Figure 3A). The observed enhancement was between 21 to 23 folds with no apparent correlation. However, the higher the molecular weight was, the lower was the polymer concentration required to reach saturation. For instance, when the highest PVP molecular weight was tested (1300K), the fluorescence signal plateaued after adding $1.75x10^{-6}$M (in polymer concentration). On the other hand, a 450 fold increase in polymer concentration was needed for the lowest PVP molecular weight (10K) to reach signal saturation (*ca.* $8x10^{-4}$ M).

This indirect correlation between the molecular weight of PVP and the saturation concentration might be explained by two interaction models; in the first model, MPS-PPV is wrapping the exterior of the PVP macromolecule spheres (Figure 3B I). As the molecular weight increases, the polymer hydrodynamic radius increases providing bigger surface area for MPS-PPV adsorption. The second model consists of intimate interactions between the conjugated polyelectrolytes and the PVP backbone (Figure 3B II). With the high polymer molecular weight, the monomer repeat units per polymer increases providing higher contact surface. To address this hypothesis, we normalized the fluorescence emission by the monomer repeat unit concentration. Figure 3C reveals that irrespective of the polymer molecular weights, all polymers saturates at

the same PVP monomer concentration at a ratio of *ca.* 150:1 (PVP:MPS-PPV). If the conjugated polymer was strictly adhering to the outer PVP sphere, the monomer ratio of PVP to MPS-PPV would increase with increasing PVP molecular weight. This finding, therefore, endorses the second proposed mechanism and reveals an intimate type of interaction between the backbones of both polymers. We speculate that this unique mode of interaction is the prime reason behind the improved photophysical properties reported herein.

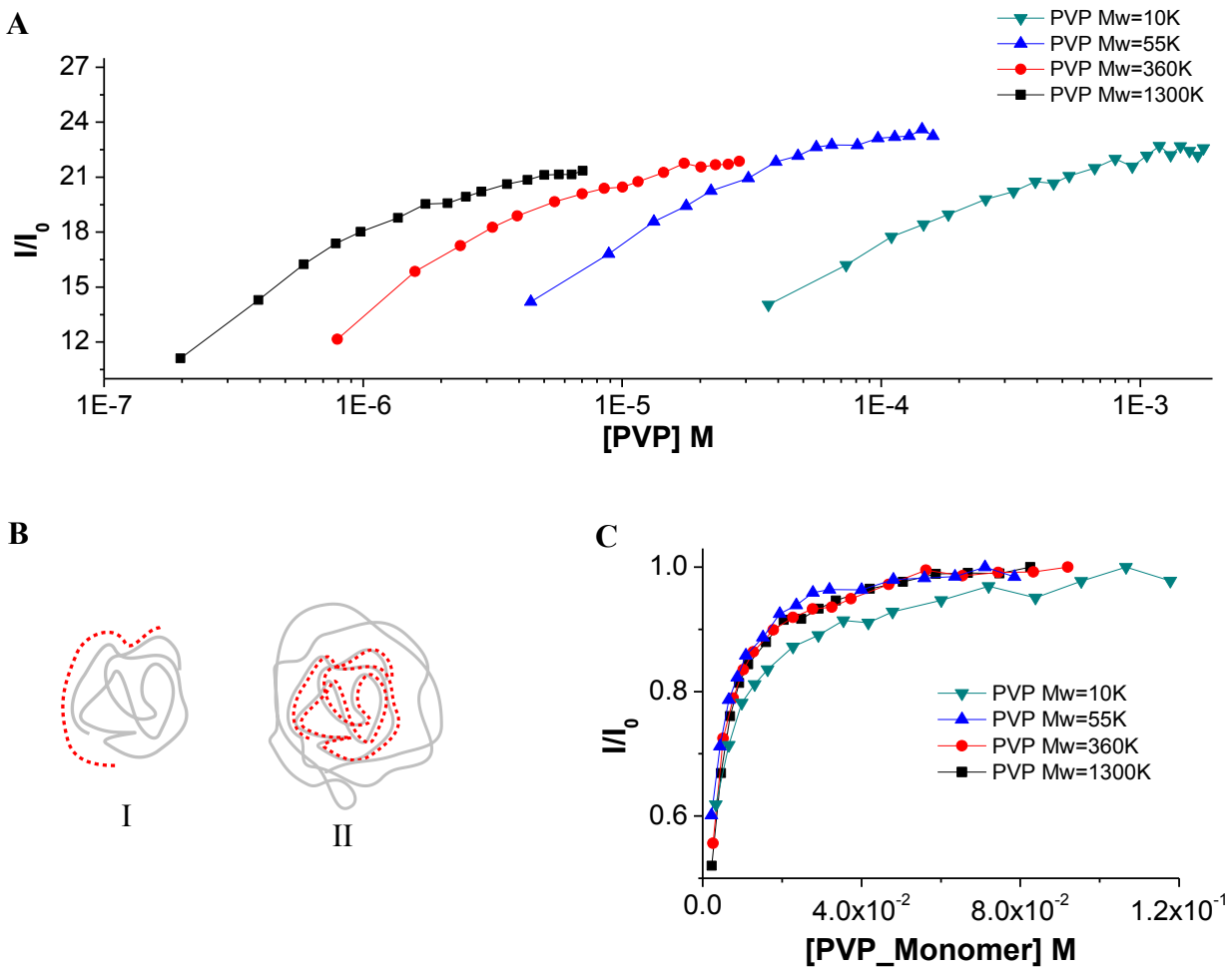

Figure 3: (A) Fluorescence enhancement versus the amphiphilic polymer concentration upon incremental addition of 10K, 55K, 360K and 1300K of PVP to an MPS-PPV solution ($1.6x10^{-4}$M reported in monomer concentration). (B) Schematic representation of the two proposed interaction models between MPS-PPV and PVP. (C) Fluorescence enhancement acquired in (A)

plotted against PVP monomer concentration. All measurements were done in 10 mM HEPES buffer pH=7.3 and 150 mM NaCl and emission spectra were acquired upon excitation at 450nm. The lines connecting the experimental points are for visual aid.

To further elucidate the mode of interaction between the two polymers, we performed a series of quenching experiments. We chose methylviologen as it has been shown to quench by electron transfer the fluorescence emission of MPS-PPV effectively.[30] Therefore unprotected segments are prone to quenching Figure 4 summarizes the stern-volmer plots obtained for the different nanohybrid structures (PVP:MPS-PPV 150:1 monomer ratio). With the exception of PVP 10K, all particles showed an unquenchable fraction (I_0/I= 1.25) reflecting that 80% of the MPS-PPV is inaccessible to MV^{2+} and buried at the core of the amphiphilic macromolecule. This result reinforces the previous conclusion. We hypothesized that the short polymer length of PVP (10K) is unable to interact with the entire MPS-PPV backbone thus exposing an additional fraction of the conjugated polymer to the quencher. On the other hand, larger PVP molecular weights (55K, 360K and 1300K) shield efficiently the MPS-PPV backbone. As a result, the unquenchable (protected) fraction is greater with larger amphiphlic polymers. Unless otherwise stated, the PVP molecular weight that will be used in the following experiments is equal to 55K.

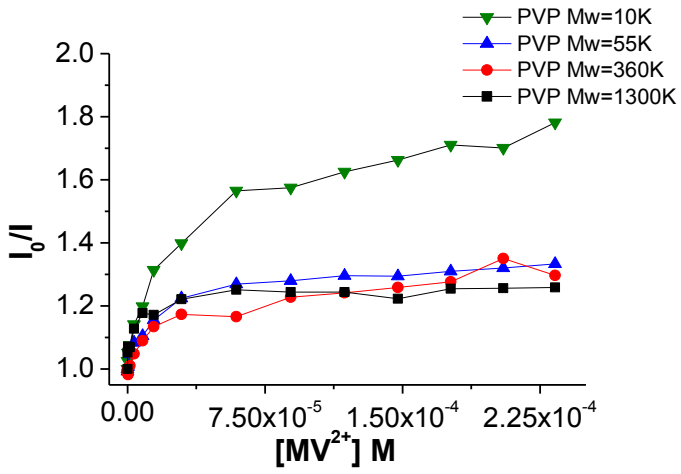

Figure 4: Stern-volmer plots for MPS−PPV/PVP nanohybrid solutions prepared with different PVP molecular weights at PVP:MPS-PPV 150:1 monomer ratio, upon adding increasing MV^{2+} concentrations. Experiments are done in 150 mM NaCl and 10 mM HEPES buffer solutions at pH=7.2. The lines connecting the experimental points are a visual aid.

Nanohybrid Photostability: We next focused our attention on evaluating the nanohybrid photostability. It was of great interest to us to prepare, in addition to a bright nanohybrid, a photostable particle that could be implemented in imaging applications and single molecule biosensing assays. Pristine conjugated polymer and nanohybrid solutions were subjected to continuous excitation at 450nm; MPS-PPV exhibited a decay over time (20% of the original intensity was lost over 10^4 seconds; Figure 5). In a marked contrast, the nanohybrid solution fluorescence intensity increased over the same time window by 18%. Nanohybrid particles prepared with different PVP molecular weights (10K and 360K in addition to 55K; SI. Fig. S.1) were tested. Both higher PVP molecular weight polymers (55K and 360K) showed similar photostability and an intensity increase of 6% within the first $4x10^3$seconds. When compared to the smallest PVP molecular weight, only a 3% increase was observed. Based on the previous quenching experiments and the image gained of the polymer-polymer interaction, we can infer that the CPE photostability is intertwined with the intimate backbone contacts of the two polymers.

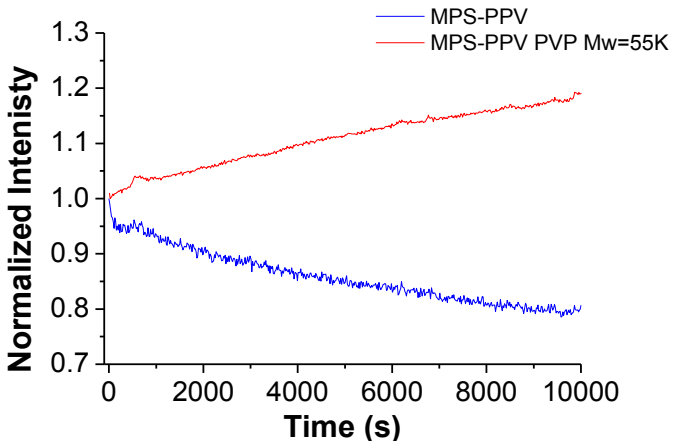

Figure 5: Intensity versus time trajectories of MPS-PPV and MPS-PPV/PVP (PVP:MPS-PPV 150:1 monomer ratio) nanohybrid upon continuous excitation at 450 nm. The experiment was done in 10 mM HEPES buffer pH=7.3 and 150 mM NaCl and emission spectra were acquired upon excitation at 450nm.

To explain why are we observing the increase in fluorescence intensity and how is PVP contributing to MPS-PPV photostability, we resorted to single particle spectroscopy experiments. We monitored individual nanohybrid fluorescence emission using a stage scanning inverted fluorescence microscope coupled to an Argon laser with continuous excitation at 488nm.

The emission was collected with a high numerical aperture objective and was directed to an avalanche photodiode detector (APD). All images showed diffraction-limited spots (*ca.* 300 nm in diameter) resulting from the emission of the nanohybrid particles (Figure 6).We then acquired intensity vs. time trajectories of single nanohybrid particles upon continuous excitation at 488 nm (Figure 7).

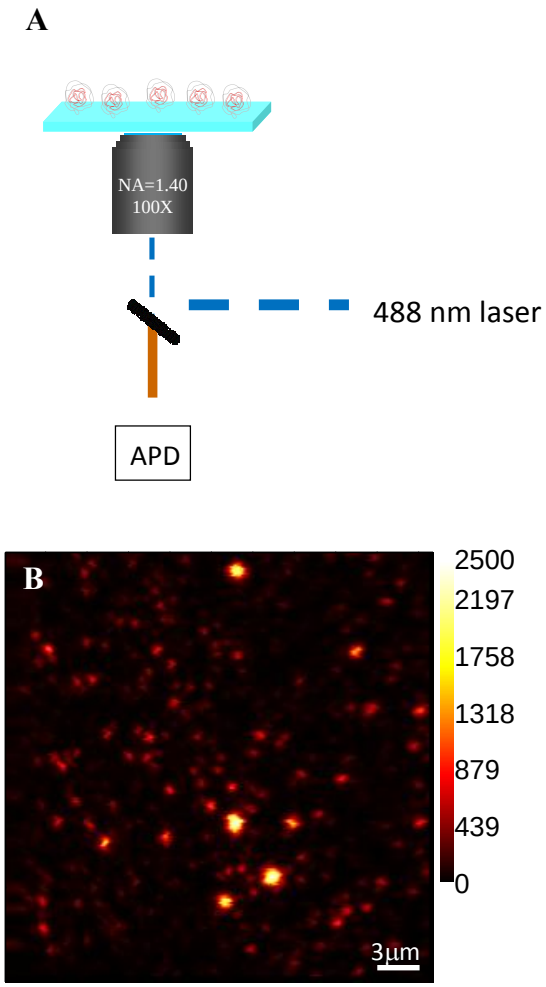

Figure 6: (A) A simplified representation of the single particle setup. (B) A 30x30 μm^2 single particle fluorescence scanning confocal image obtained upon 488 nm excitation of the nanohybrid structure prepared at PVP:MPS-PPV 150:1 monomer ratio. The right bar illustrates the counts per millisecond per pixel.

None of the recorded traces showed a sign of blinking which is highly beneficial for real-time single particle tracking. The resulting trajectories can be categorized into three distinctive patterns. 16 % showed no change in intensity and only 9% showed exponential photodegradation. The majority (75% of all recorded traces) however showed an initial increase

in the intensity followed by a steady decrease (Figure 8). On average, the intensity increased by 1.8 folds within the first 31 seconds (SI Fig S.2). After 4 minutes of continuous excitation, we observed, on average, only an 18% decrease from the original intensity. [47] Similar pattern has been previously observed by McGniel *et al.* at the ensemble level when conjugated nanodots made of poly(2,5-di(3=,7=-dimethyloctyl)phenylene-1,4-ethynylene where continuously excited.[48] The fluorescence intensity peaked at around 4 minutes before it started to decrease.

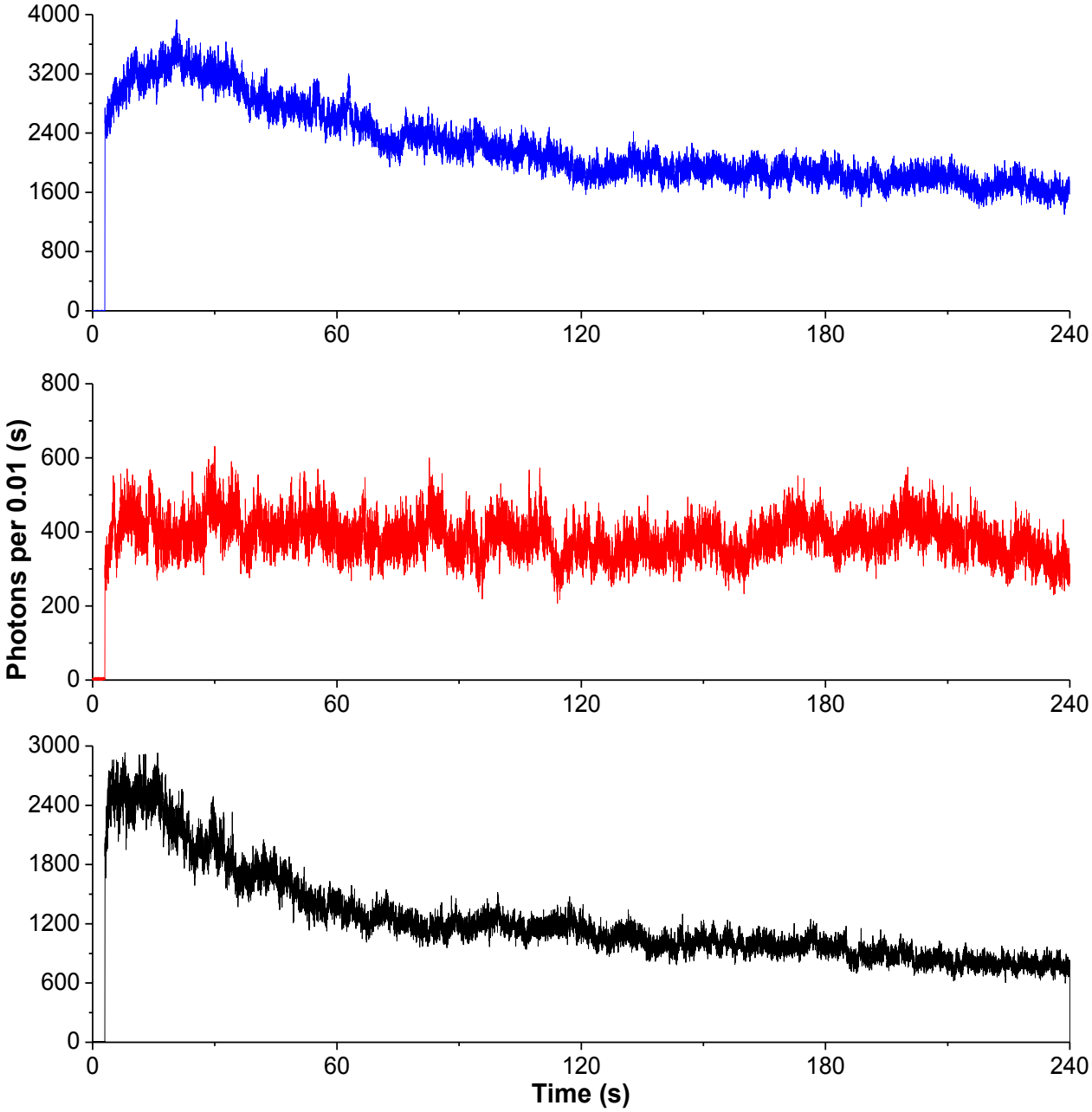

Figure 7: Intensity-time trajectories of the single particle nanohybrid acquired upon 488-nm excitation. The three traces represent the three different categories of the intensity change over time.

To explain this unique behavior, we tested few hypothesis; we first argued that this increase is due to conformation restructuring and energy minimization between the two polymers leading to

an increase in backbone extension /stabilization of the system over time. Given that the single particle traces were sequentially acquired with a time difference of few hours between some traces, the first hypothesis was quickly dropped.

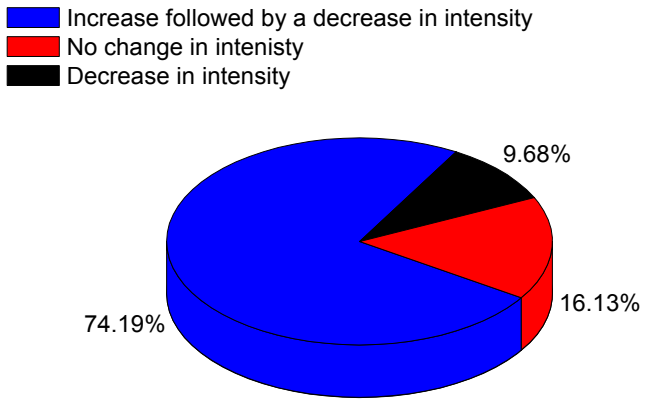

Figure 8: Statistical distribution of the intensity-time trajectories of the single particle nanohybrid.

We then considered the probability that polymer restructuring is catalyzed by the thermal energy provided by the focused excitation beam. Indeed, a nanohybrid solution showed a 16% increase in fluorescence intensity after 5 mins incubation at 35^0C (SI Fig S.3). However, based on theoretical calculations reported by Hell *et al.,* the temperature increase under our experimental conditions would not exceed 0.2-0.3K.[49] In addition, the glass coverslip onto which the nanohybrid is deposited would act as an efficient heat sink.

The inherited complex photophysics of conjugated polyelectrolytes in addition to the strong backbone-backbone interaction with PVP might hold the answer to this unusual behavior. Individual conjugated polyelectrolyte polymer, as stated earlier, could be described as a chain of multiple connected chromophores. In a highly concentrated solution of fluorophores, given the short distance between molecules, intermolecular Förster resonance energy transfer may occur leading to efficient self-quenching. Over time, and upon photodegradation, the active fluorescent molecule concentration decreases leading to an increase in the fluorescent signal. In a similar fashion, photodegradation of the highly concentrated chromophores per polymer chain reduces the number of emissive sites leading to "chromophore dilution" over time. As a result, quenching by energy transfer is dramatically reduced leading to the observed fluorescent enhancement. Upon continues irradiation, the chromophore reaches a tipping point where the enhancement by the dilution effect is overtaken by its continuous photodestruction. This eventually results in the gradual decrease in the fluorescence intensity of the single nanohybrid particle.

The amount of photons emitted, on average, per trace within our experimental window (240 s) was equal to 1.85 $x10^9$ (None of the recorded traces did completely photobleach only 18% of the original intensity was lost on average*).* This amount of emitted photons is one the highest reported so far and by far better than freely floating MPS-PPV.[26] When compared to other organic fluorophores, Cy5, for instance, would emit $6.5x10^5$ photons before irreversible photobleaching and Alexa 633 around $9.3x10^6$.[50] Conjugated polymer dots prepared from conjugated polymers were reported to emit between 10^6 and 10^9 before complete irreversible photobleaching. [48, 51]

CPE photostability in general is attributed to the protection from molecular oxygen provided by surfactants.[38] However, in our specific case, PVP macromolecules are known to be oxygen

permeable.[52, 53] In a recent single molecule study, Scheblykin *et al.* showed that the collision between freely diffusing conjugated polymers lead to the simultaneous rupture of polymer chains.[54] The mechanical bending of the stiff conjugated macromolecules upon impact can weaken the chemical bond and markedly catalyze the photochemical oxygen reaction at the contact point. This in turn accelerates chain degradation by at least 20 times. In addition, chain bending was found to be also accentuated by prolonged polymer backbone interaction. Based on the previously discussed molecular interaction, we believe that the intimate backbone interactions between PVP and the anionic conjugated polyelectrolyte is providing a protective shell against interchain impact and inhibiting prolonged backbone interactions thus increasing the photostability of the conjugated polyelectrolyte. It also explains why the short PVP (10K) did not protect, as efficiently, the CPE from photodegradation.

Tuning the fluorescent intensity of the nanohybrid particles: Based on all the previous results and the acquired molecular understanding of the interaction between MPS-PPV and PVP, we speculated that the intensity of the nanohybrid particles could be tuned by modifying the order of addition (Figure 9). When MPS-PPV is added to a solution of PVP, the amphiphilc macromolecules will compete to complex with the newly added MPS-PPV resulting in a homogenous distribution of CPEs among the nanohybrid particles (Sample 1). However, When PVP is added to a solution of MPS-PPV, the first amphiphilic macromolecules will be exposed to a large amount of anionic CPEs. Consequently, each PVP polymer will scavenge multiple CPEs (Sample 2). To verify our hypothesis, we examined the two samples at the single particle level.

As described earlier, single particle confocal images were acquired. Fluorescence intensities were calculated for each particle and their distributions are summarized in Figure 9B. When PVP

is added to MPS-PPV, the average photon count per particle was equal to 683 with a standard deviation of 147. The other order of addition yielded an average of photon count per particle of 275 with a standard deviation of 91. As expected, the addition of PVP to a solution of MPS-PPV (rather than the addition of MPS-PPV to PVP) generates brighter MPS-PPV/PVP hybrids. This result offers a simple way to tune the nanohybrid particle intensity.

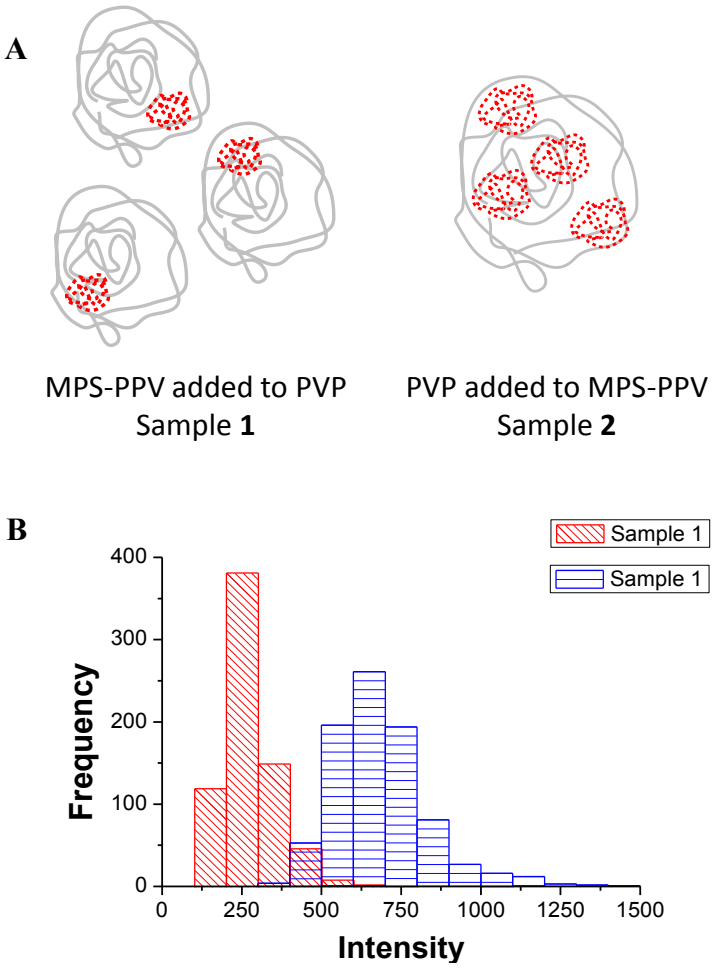

Figure 9: (A) Schematic illustration of a potential interaction of MPS-PPV in complex with PVP based on the order of addition. (B) Intensity distribution histograms extracted from single particle confocal images of sample 1 and sample 2.

Conclusion: We report herein a straightforward method to prepare photostable, bright and none blinking nanohybrid particles by complexing an anionic conjugated polyelectrolytes with PVP. By employing ensemble and single particle spectroscopy methods, we unraveled the mode of interaction between the two polymers, quantified the amount of photon emitted per particle and explained the mechanism behind its photostability. The fluorescence intensity can be easily tuned by simply changing the order of addition. It is therefore possible to tune the particle brightness by using different PVP molecular weights. Given the unique and improved photostability, the nanohybrid particles can prove instrumental in current state-of-the-art single molecule tracking, bioimaging and single molecule/particle based sensing assays.

Methods:

Chemicals: poly[5-methoxy-2-(3-sulfopropoxy)-1,4-phenylenevinylene]potassiumsalt(MPS-PPV), HEPES sodium salt, polyvinylpyrrolidone(Average Mw 10K; 55K; 360K; 1,300K), Methyl viologen dichloride hydrate 98% were purchased from Sigma-Aldrich.

Absorption and Emission Spectrum: Steady-state fluorescence spectroscopy was carried out using a Thermo Scientific Lumina spectrophotometer. Absorption spectra were recorded using a Jasco V-570 UV−vis spectrophotometer in double-beam mode. For all steady-state absorption and emission experiments, the solutions were placed in 1 cm × 1 cm quartz cuvettes.

Quenching Experiments: Concentrated solutions of methyl viologen were prepared on the same day of the quenching experiment. Aliquots of methyl viologen in 150 mM NaCl, 10 mM

HEPES, pH 7.2-7.4 were added to the samples, and fluorescence spectra were taken immediately after mixing.

Single Molecule Experiments: Sample preparation: glass coverslips were cleaned in a piranha solution (15: 5 mL H_2SO_4:H_2O_2) for 1 hour. Flow chambers were prepared with a predrilled polycarbonate film (GraceBio) with an adhesive gasket which was assembled on top of the cleaned surface yielding a chamber with a total volume of 10 μL. Nano-hybrid particles in the concentratin range of 10^{-9} M were injected into the chanber. All experiments were run under a constant flow of an oxygen scavenger solution consisting of β-mercaptoethanol 1% v/v, β-D(+)glucose 3% w/v, glucose oxidase 0.1 mg/mL, and catalase 0.02 mg/mL. Solutions were 10 mM in HEPES buffer pH 7.3 and 150 mM in NaCl. All experiments were conducted at room temperature (22-23 °C).

Confocal Imaging: The experimental setup consisted of an Olympus IX-71 inverted microscope operated in a confocal form and provided with a closed-loop sample scanning stage (Nano LP100, Mad City Labs, Madison, WI) used for imaging and sample positioning. Samples were excited continuously employing the 488 nm (53 $W.cm^{-2}$) from output from an Ar+ laser. The circularly polarized laser beam was introduced via a single mode fiber optic and directed by a dichroic beamsplitter (z488rdc DCLP, Chroma, Rockingham, VT) to the sample via a high numerical aperture (NA = 1.40) oil immersion objective (Olympus U PLAN SAPO 100X). Fluorescence emission was collected through the same objective and then directed to an avalanche photodiode detector (PerkinElmer Optoelectronics SPCM-AQR-14, Vaudreuil, Quebec, Canada). The emission was cleaned from any residual laser excitation by an HQ500LP (from Chroma, Rockingham, VT). Images consisting of 256 by 256 pixels were acquired by collecting the intensity for 1 ms at each pixel. Intensity-time trajectories were recorded at 1 ms

dwell time by positioning the stage on a single nanohybrid particle. A home built LabView routine was used for data acquisition and stage positioning. A National Instruments NI-PCI-6602 board was used as a counter board.

Supplementary Information. Dynamic light scattering, Photostability of different nanohybrids, and emission and absorption spectrum are available in the supporting information.

AUTHOR INFORMATION

Corresponding Author

*To whom correspondence should be addressed:
Phone: 961-1-350000 Ext 3989 **Fax:** 961-1-350000 Ext 3970 **Email:** pk03@aub.edu.lb

Funding Sources

TWAS (Award number: 12-316 RG/MSN/AF/AC_C; UNESCO FR 3240270863) and the University research board (Award number: 102848)

ACKNOWLEDGMENT

The authors are grateful to Dr. Gonzalo Cosa's Laboratory at McGill University for providing access to their single molecule spectroscopy setup. This work was supported by TWAS (Award number: 12-316 RG/MSN/AF/AC_C; UNESCO FR 3240270863) and the University research board (Award number: 102848)

REFERENCES

1. A. T. Ngo, P. Karam and G. Cosa, *Pure and Applied Chemistry*, 2010, **83**, 43-55.
2. H. Jiang, P. Taranekar, J. R. Reynolds and K. S. Schanze, *Angewandte Chemie International Edition*, 2009, **48**, 4300-4316.
3. J. H. Seo, A. Gutacker, Y. Sun, H. Wu, F. Huang, Y. Cao, U. Scherf, A. J. Heeger and G. C. Bazan, *Journal of the American Chemical Society*, 2011, **133**, 8416-8419.
4. Z. He, C. Zhong, S. Su, M. Xu, H. Wu and Y. Cao, *Nature Photonics*, 2012, **6**, 591-595.
5. Z. He, C. Zhong, X. Huang, W. Y. Wong, H. Wu, L. Chen, S. Su and Y. Cao, *Advanced Materials*, 2011, **23**, 4636-4643.

6. L. Lu, F. H. Rininsland, S. K. Wittenburg, K. E. Achyuthan, D. W. McBranch and D. G. Whitten, *Langmuir*, 2005, **21**, 10154-10159.
7. P. Karam, A. A. Hariri, C. F. Calver, X. Zhao, K. S. Schanze and G. Cosa, *Langmuir*, 2014, **30**, 10704-10711.
8. K. Ogawa, S. Chemburu, G. P. Lopez, D. G. Whitten and K. S. Schanze, *Langmuir*, 2007, **23**, 4541-4548.
9. S. Chemburu, E. Ji, Y. Casana, Y. Wu, T. Buranda, K. S. Schanze, G. P. Lopez and D. G. Whitten, *The Journal of Physical Chemistry B*, 2008, **112**, 14492-14499.
10. K. Achyuthan, T. Bergstedt, L. Chen, R. Jones, S. Kumaraswamy, S. Kushon, K. Ley, L. Lu, D. McBranch and H. Mukundan, *Journal of Materials Chemistry*, 2005, **15**, 2648-2656.
11. D. Wang, X. Gong, P. S. Heeger, F. Rininsland, G. C. Bazan and A. J. Heeger, *Proceedings of the National Academy of Sciences*, 2002, **99**, 49-53.
12. J. Liang, K. Li and B. Liu, *Chemical Science*, 2013, **4**, 1377-1394.
13. M. R. Pinto and K. S. Schanze, *Proceedings of the National Academy of Sciences of the United States of America*, 2004, **101**, 7505-7510.
14. C. Tan, M. R. Pinto and K. S. Schanze, *Chemical Communications*, 2002, 446-447.
15. S. W. Thomas, G. D. Joly and T. M. Swager, *Chemical Reviews*, 2007, **107**, 1339-1386.
16. Q. Zhou and T. M. Swager, *Journal of the American Chemical Society*, 1995, **117**, 7017-7018.
17. B. S. Gaylord, A. J. Heeger and G. C. Bazan, *Proceedings of the National Academy of Sciences*, 2002, **99**, 10954-10957.
18. B. S. Gaylord, A. J. Heeger and G. C. Bazan, *Journal of the American Chemical Society*, 2003, **125**, 896-900.
19. B. Liu and G. C. Bazan, *Chemistry of materials*, 2004, **16**, 4467-4476.
20. X. Zhao, Y. Liu and K. S. Schanze, *Chemical Communications*, 2007, 2914-2916.
21. L. Chen, D. W. McBranch, H.-L. Wang, R. Helgeson, F. Wudl and D. G. Whitten, *Proceedings of the National Academy of Sciences*, 1999, **96**, 12287-12292.
22. A. Duarte, A. Chworos, S. F. Flagan, G. Hanrahan and G. C. Bazan, *Journal of the American Chemical Society*, 2010, **132**, 12562-12564.
23. P. A. Dalgarno, C. A. Traina, J. C. Penedo, G. C. Bazan and I. D. W. Samuel, *Journal of the American Chemical Society*, 2013, **135**, 7187-7193.
24. K.-Y. Pu and B. Liu, *Advanced Functional Materials*, 2011, **21**, 3408-3423.
25. T. Huser, M. Yan and L. J. Rothberg, *Proceedings of the National Academy of Sciences*, 2000, **97**, 11187-11191.
26. P. Karam, A. T. Ngo, I. Rouiller and G. Cosa, *Proceedings of the National Academy of Sciences*, 2010, DOI: 10.1073/pnas.1008068107.
27. M. Yan, L. Rothberg, F. Papadimitrakopoulos, M. Galvin and T. Miller, *Physical review letters*, 1994, **73**, 744.
28. .
29. G. A. Montano, A. M. Dattelbaum, H.-L. Wang and A. P. Shreve, *Chemical Communications*, 2004, DOI: 10.1039/b401682c, 2490-2491.
30. A. T. Ngo and G. Cosa, *Langmuir*, 2009, **26**, 6746-6754.
31. A. T. Ngo, P. Karam, E. Fuller, M. Burger and G. Cosa, *Journal of the American Chemical Society*, 2008, **130**, 457-459.
32. Y. Liu, K. Ogawa and K. S. Schanze, *Analytical Chemistry*, 2007, **80**, 150-158.

33. M. L.-Viger, D. Brouard and D. Boudreau, *The Journal of Physical Chemistry C*, 2011, **115**, 2974-2981.
34. S. H. Lee, S. Kömürlü, X. Zhao, H. Jiang, G. Moriena, V. D. Kleiman and K. S. Schanze, *Macromolecules*, 2011, **44**, 4742-4751.
35. D.-L. Jiang, C.-K. Choi, K. Honda, W.-S. Li, T. Yuzawa and T. Aida, *Journal of the American Chemical Society*, 2004, **126**, 12084-12089.
36. J.-M. Koenen, X. Zhu, Z. Pan, F. Feng, J. Yang and K. S. Schanze, *ACS Macro Letters*, 2014, **3**, 405-409.
37. R. D. Scurlock, B. Wang, P. R. Ogilby, J. R. Sheats and R. L. Clough, *Journal of the American Chemical Society*, 1995, **117**, 10194-10202.
38. W. Dou, C. Wang, G. Wang, Q. Ma and X. Su, *The Journal of Physical Chemistry B*, 2008, **112**, 12681-12685.
39. H.-W. Liu, A. T. Ngo and G. Cosa, *Journal of the American Chemical Society*, 2011, **134**, 1648-1652.
40. V. P. Torchilin, T. S. Levchenko, K. R. Whiteman, A. A. Yaroslavov, A. M. Tsatsakis, A. K. Rizos, E. V. Michailova and M. I. Shtilman, *Biomaterials*, 2001, **22**, 3035-3044.
41. J. Huang, L. H. Bu, J. Xie, K. Chen, Z. Cheng, X. G. Li and X. Y. Chen, *ACS Nano*, 2010, **4**, 7151-7160.
42. H. Y. Lee, A. Y. Seol, K. H. Jeong and Y. J. Kim, *Macromolecular Research*, 2007, **15**, 547-552.
43. H. Kamada, Y. Tsutsumi, Y. Yamamoto, T. Kihira, Y. Kaneda, Y. Mu, H. Kodaira, S.-i. Tsunoda, S. Nakagawa and T. Mayumi, *Cancer research*, 2000, **60**, 6416-6420.
44. U. Resch-Genger, M. Grabolle, S. Cavaliere-Jaricot, R. Nitschke and T. Nann, *Nature methods*, 2008, **5**, 763-775.
45. S. Tretiak, A. Saxena, R. Martin and A. Bishop, *Physical review letters*, 2002, **89**, 097402.
46. R. Godin, R. E. Palacios and G. Cosa, *The Journal of Physical Chemistry C*, 2015, **119**, 12875-12886.
47. .
48. C. Wu, B. Bull, C. Szymanski, K. Christensen and J. McNeill, *ACS Nano*, 2008, **2**, 2415-2423.
49. A. Schönle and S. W. Hell, *Opt. Lett.*, 1998, **23**, 325-327.
50. T. Schmidt, U. Kubitscheck, D. Rohler and U. Nienhaus, *Single Molecules*, 2002, **3**, 327-327.
51. C. Wu, C. Szymanski, Z. Cain and J. McNeill, *Journal of the American Chemical Society*, 2007, **129**, 12904-12905.
52. J. Wichterlová, K. Wichterle and J. Michálek, *Polymer*, 2005, **46**, 9974-9986.
53. J. Hadassah and P. K. Sehgal, *Clinical and Experimental Optometry*, 2006, **89**, 374-380.
54. Y. Tian, M. V. Kuzimenkova, M. Xie, M. Meyer, P.-O. Larsson and I. G. Scheblykin, *NPG Asia Mater*, 2014, **6**, e134.

Nanohybrid Conjugated Polyelectrolytes: Highly Photostable and Ultrabright Nanoparticles

*Ghinwa H. Darwish, Pierre Karam**

Department of Chemistry, American University of Beirut, P.O. Box 11-0236, Beirut, Lebanon

KEYWORDS: Conjugated polyelectrolytes, Photostability, Fluorescent enhancement, MPS-PPV, polyvinylpyrrolidone , Single Molecule Spectroscopy.

We present a general and straightforward one-step approach to enhance the photophysical properties of conjugated polyelectrolytes. Upon complexation with an amphiphilic polymer (polyvinylpyrrolidone), an anionic conjugated polyelectrolyte (Poly[5-methoxy-2-(3-sulfopropoxy)-1,4phenylenevinylene]) was prepared into small nanoparticle with exceptional photostability and brightness. The polymer fluorescence intensity was enhanced by 23 folds and could be easily tuned by changing the order of addition. Single molecule experiments revealed a complete suppression of blinking. In addition, after only losing 18% of the original intensity, a remarkable amount of photons were emitted per particle (~10^9, on average). This number is many folds greater than popular organic fluorescent dyes. We believe an intimate contact between the two polymers is shielding the conjugated polyelectrolyte from the destructive photooxidation. The prepared nanohybrid particles will prove instrumental in single particle based fluorescent assays and can serve as a probe for current state-of-the-art bioimaging fluorescent techniques.

Conjugated polyelectrolytes (CPEs) are remarkable materials with enormous range of applications.[1, 2] They have been implemented in cheap organic solar cells,[3-5] and as new promising class of antibacterial agents[6] and were recently used as efficient fusiogenic materials.[7] They were particularly useful in developing single particle based bio- and chemical sensing assays.[1, 8-12] CPEs can detect the presence of fluorescent quenchers with exquisite and amplified sensing capabilities.[13-16] As such, they were successfully used to sense specific oligonucleotides sequences,[11, 17-19] small molecules,[20] biomolecules[21] and discriminate between different bacteria strains.[22] Given their low cytotoxicity, compared to quantum dots, numerous attempts were geared towards developing them into targeted fluorescent probes for cell imaging applications.[23, 24]

Despite their huge potentials, they still suffer from blinking, fast irreversible photobleaching and low quantum yield efficiency. This has therefore limited their wide spread implementation into long shelf life sensing devices and probes for bioimaging and single particle tracking applications. Such techniques require exceptional photostability and brightness to obtain significant spatial and temporal information on the target or the cellular and subcellular structures they probe. It took laborious ensemble and single-molecule spectroscopy studies to understand and improve CPEs photophysical properties.[14, 25, 26]

CPEs backbones are prone to chemical oxidation by singlet oxygen leading to the creation of a permanent photochemical defects that quenches their excitations.[27] Their fluorescence emission originates from individual chromophores presumably delimited by twists that breaks the π–π orbitals delocalization and creates multiple emissive sites.[28] As such, polymer photophysics strongly correlates with its backbone conformation and its solvated state.[25] It dictates the energy transfer efficiency between neighboring chromophores. For instance, in water, conjugated

polyelectrolytes adopt a highly coiled conformation to minimize the interaction between its hydrophobic backbone and the nonpolar solvent. The collapsed state induces stresses along the backbone leading to the formation of kinks and defective sites, which can serve as trapping and nonradiative recombination sites. The aggregated state also results in the formation of shorter chromophores and long range ordered and highly packed chains thus favoring efficient interchain or through-space energy transfer, which strongly compete with radiative emission processes.[24] The combined effects result in low quantum yield and overall mediocre photophysical properties in water as compared to other nonpolar solvents. Specifically, recent single molecule studies demonstrated this direct correlation between the CPE conformation/solvation state and its spectroscopic properties.[26] When anionic conjugated polyelectrolyte, poly[5-methoxy-2-(3-sulfopropoxy)-1,4-phenylene-vinylene] (MPS-PPV), is encapsulated in negatively charged liposomes, it exists in a freely diffusing yet as a collapsed state. Discrete fluorescence intensity levels and individual on-off transition steps were reported in the single-particle fluorescence intensity-time trajectories. This quantized behavior reflects the efficient interchain exciton transport to localized fluorescence quenching sites along the PPV backbone (oxidation, kinks etc). In marked contrast, extended polymer chains embedded within the lipid membranes showed exponential decrease in intensity over time. This behavior is characteristic of the photobleaching of a collection of multiple independent chromophores. When compared to the aggregated/collapsed structure, the relatively extended CPEs showed brighter intensities and better photostability.

Building on the knowledge gained from steady state fluorescent experiments and single molecule studies, polyelectrolytes and surfactants were used to facilitate CPEs solubility and favor backbone disaggregation. [7, 29, 30] In return, these structures provided enhanced fluorescence

performance with excellent sensing capabilities down to the single molecule level.[9, 31, 32] Other approaches employed metal enhanced fluorescence methods to increase the CPE quantum yield from, for instance, 3 to 77% by positioning a polythiophene conjugated polymer close to a spherical silver nanoparticle separated by a silica spacer.[33]

The presence of specific surfactants and metallic nanoparticles, however, limited the application of CPEs. New strategies to disaggregate the polymer have emerged by deliberately engineering the polymer side chains and its backbone.[34] PPE-based conjugated polyelectrolytes were modified with dendritic poly(benzyl ether) terminated with carboxylic acid groups as side chains.[35] With each dendrimer generation, the backbone charge density increased, resulting in its disaggregation and subsequent increase in its fluorescence quantum yield. Recently, a more surgical approach was reported; the oxygen atom directly connected to the phenylene rings in a PPE-based CPE was substituted with a carbon atom.[36] This modification suppressed the tendency of the polymer to aggregate in water and the quantum yield increased from 4 to 16%. However, these modifications remain specific to a narrow class of conjugated polyelectrolytes.

CPEs also suffer from low photostability due to the destructive effect of singlet oxygen.[37] In some cases, the addition of surfactants shielded the conjugated backbone from oxygen. [38] Additives did also improve on the polymer photophysics. Liu *et al.* have reported on the healing effect of β-mercaptoethanol (BME), a known antioxidant, on photooxidated CPE.[39] Although BME was able to recover the fluorescence loss of CPEs for multiple cycles, it did not prevent the photodegradation of CPEs.

Consequently, there exists a major challenge to improve CPEs fluorescent efficiency and photostability while increasing their functionality. Previous attempts introduced stringent

conditions that often narrowed the CPE spectrum of applications. In this work, we report a straightforward and a general approach to increase the fluorescence quantum yield and, most importantly, enhance the photostability of a commercially available conjugated polyelectrolyte MPS-PPV. Polyvinylpyrrolidone (PVP), an amphiphilic polymer, was used as a scaffold to extend the polymer backbone and protect it from photodegradation which resulted in a 23 folds increase in its quantum efficiency. Single particle studies revealed the emission of a remarkable number of photons per particle. On average, 10^9 photons were emitted when the fluorescent signal was only 18% down from its initial intensity. All traces showed no sign of blinking during our experiment time window. The prepared hybrid particles were estimated to be in the range of few nm in diameters (*ca.* hydrodynamic 15-20nm). In this report, we will address fundamental questions such as how is PVP protecting the vulnerable CPE from photodegradation and how is it enhancing its photophysical properties? Our findings are significant, as they present a facile approach to prepare bright and highly photostable conjugated polyelectrolytes.

Results and Discussions:

Hybrid nanoparticle design: In this study, we used the anionic Poly[5-methoxy-2-(3-sulfopropoxy)-1,4phenylenevinylene] (MPS-PPV) (Figure 1A) as a surrogate/model system to investigate the effect of an amphiphilic macromolecule on improving the photophysical properties of CPEs. MPS-PPV is commercially available and has been extensively used as a platform for biosensing schemes. In addition, its photophysical properties have been studied at the ensemble and single molecule levels.[26, 30, 39]

Our strategy was to search for an amphiphilic macromolecule that would disaggregates the hydrophobic backbone of MPS-PPV through strong and stable complexation/interactions

contacts. Consequently, this will allow us to efficiently dissolve and extend the polymer backbone, and enhances its water solubility and photophysical properties. The macromolecule, in addition, should be readily modified to indirectly introduce chemical functionality to existing conjugated polyelectrolytes. To fulfill these purposes, we chose polyvinylpyrrolidone (PVP) (Figure 1B) which is considered a safe material and has been approved by FDA for many medical uses. PVP has been extensively used to prepare biocompatible nanoparticles, drug delivery vehicles and passivate biomaterial surfaces.[40, 41] It could be also prepared with a terminal primary amine or a carboxylic acid group.[42, 43] Specific biomolecules or small organic molecules of interest could be then introduced. This in turn adds an array of potential functionality and applications to the prepared hybrid structure while avoiding the complexity that accompanied the direct CPEs chemical modifications.

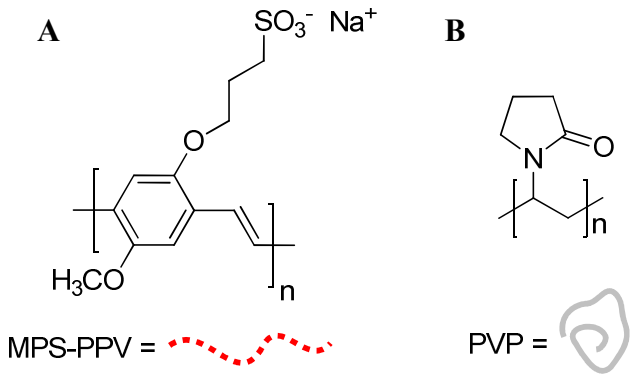

Figure 1: Chemical structures and their equivalent cartoon representations of (A) the anionic conjugated polyelectrolyte Poly[5-methoxy-2-(3-sulfopropoxy)-1,4phenylenevinylene] sodium (MPS-PPV) and (B) the amphiphilic macromolecule polyvinypyrolidone (PVP).

The hybrid particles were prepared by mixing a solution of MPS-PPV with different molecular weights of PVP. We characterized the particles by performing light scattering experiments. Particles size distribution (table 1, SI), revealed an average hydrodynamic diameter in the

nanosize range between 15nm - 20 nm. When compared to PVP alone, we observed an increase in the average diameter for each respective hybrid particle. Given their size, the prepared structure will be therefore referred to as "nanohybrid particle(s)". Of importance, the prepared particles were stable in solution for weeks without any signs of aggregation or precipitation.

Fluorescent Enhancement: To probe the interactions between the CPE and the amphiphilic polymer, we monitored the spectroscopic properties of MPS-PPV with and without PVP (55K). We followed the changes in MPS-PPV fluorescent emission when adding incremental amounts of the amphiphilic polymer. The enhancement was calculated as the ratio of the maximum emission intensity recorded after each addition of PVP to that of the pristine MPS-PPV (Figure 2 A). A 23-fold increase in fluorescent enhancement is observed followed by a plateau at approximately $5x10^{-5}$M in amphiphilic polymer concentration. The enhancement is ascribed to the deaggregation of the conjugated polymer backbone upon PVP complexation. As a result, the isolated chains inhibit efficient interchain coupling suppressing the possible self-quenching pathway. This strong interaction is presumably to be driven by a combination of hydrophobic contacts between the two polymer backbones, and by favorable entropy changes upon release of interfacial water molecules. The photoluminescence quantum yield of the hybrid structure was calculated to be equal to 23%. The brightness of the prepared hybrid structure was found to be equal to 420, which is significantly larger than most organic fluorescent dyes (typical reported values are <90).[44] Limited brightness of conventional dyes often results in low signal-to-background and is considered a major hurdle in sensing and single molecule fluorescence experiments.

Contrary to earlier reports, where a blue shift in the fluorescence emission was observed upon conjugated polyelectrolytes deaggregation, our results show a red shift (ca. 520 to 550 nm) thus

revealing a different interaction mechanism (Figure 2B). It was argued in previous reports that upon polymer backbone deaggregation exciton funneling to lower energy sites (red chromophores) and quenching sites can be dramatically inhibited. As such, fluorescence enhancement is often accompanied by a blue shift in the emission spectrum.

In our specific case, while the previous hypothesis still applies, it is reasonable to assume that the red shift is due to the increase in chromophore conjugation length, a phenomenon that is observed with increasing oligomer conjugation length.[45] We reasoned that upon PVP complexation, MPS-PPV chromophore length increases as a result of the suppression of the torsional motion. Interchain energy transfer to quenching sites, as expected, is also reduced. This will lead to the observed fluorescent enhancement and red-shift in the fluorescence emission spectra. In addition, the presence of PVP induced a 20 nm red shift in the CPE maximum absorbance concomitant with a slight increase in its absorbance (Figure 2C). This shift in absorbance confirms the formation of extended chromophores (i.e. red species).[45] Very recently, a report by Godin *et al.* described the fluorescent enhancement of MPS-PPV prepared in different solvent mixtures (H_2O/THF).[46] In low water content, nanoparticles (110-212 nm) exhibited a red-shift in the emission which was also attributed to the increase in conjugation length of MPS-PPV.

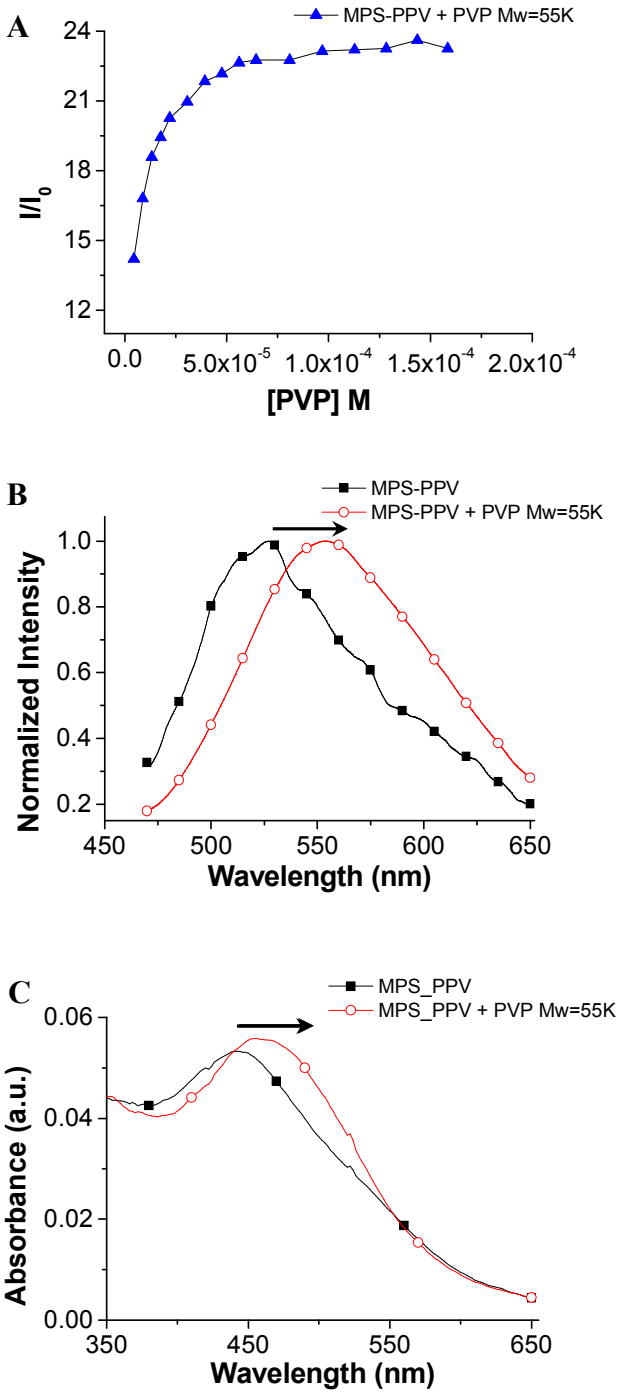

Figure 2: (A) Fluorescence emission enhancement of MPS-PPV ($1.6x10^{-4}$M in monomer concentration) upon addition of incremental amounts of PVP (MW=55K). The fluorescence ratio was calculated by dividing the maximum intensity after each addition to the maximum fluorescence emission of pristine MPS-PPV. The lines connecting the experimental points are for

visual aid. (B) Normalized fluorescence intensity and (C) absorbance spectra of pristine MPS-PPV and MPS-PPV_PVP. The polymer concentrations are: MPS-PPV=$1.6x10^{-4}$M (reported in monomer concentration) and PVP =$5x10^{-5}$M (reported in polymer concentration). All measurements were done in 10 mM HEPES buffer pH=7.3 and 150 mM NaCl and emission spectra were acquired upon excitation at 450nm.

Polymer-Polymer interaction: To gain an insight on the PVP/CPE interaction, we examined the effect of PVP molecular weight on the fluorescence enhancement. Four different molecular weights were tested and compared 10K, 55K, 360K and 1300K (Figure 3A). The observed enhancement was between 21 to 23 folds with no apparent correlation. However, the higher the molecular weight was, the lower was the polymer concentration required to reach saturation. For instance, when the highest PVP molecular weight was tested (1300K), the fluorescence signal plateaued after adding $1.75x10^{-6}$M (in polymer concentration). On the other hand, a 450 fold increase in polymer concentration was needed for the lowest PVP molecular weight (10K) to reach signal saturation (*ca.* $8x10^{-4}$ M).

This indirect correlation between the molecular weight of PVP and the saturation concentration might be explained by two interaction models; in the first model, MPS-PPV is wrapping the exterior of the PVP macromolecule spheres (Figure 3B I). As the molecular weight increases, the polymer hydrodynamic radius increases providing bigger surface area for MPS-PPV adsorption. The second model consists of intimate interactions between the conjugated polyelectrolytes and the PVP backbone (Figure 3B II). With the high polymer molecular weight, the monomer repeat units per polymer increases providing higher contact surface. To address this hypothesis, we normalized the fluorescence emission by the monomer repeat unit concentration. Figure 3C reveals that irrespective of the polymer molecular weights, all polymers saturates at

the same PVP monomer concentration at a ratio of *ca.* 150:1 (PVP:MPS-PPV). If the conjugated polymer was strictly adhering to the outer PVP sphere, the monomer ratio of PVP to MPS-PPV would increase with increasing PVP molecular weight. This finding, therefore, endorses the second proposed mechanism and reveals an intimate type of interaction between the backbones of both polymers. We speculate that this unique mode of interaction is the prime reason behind the improved photophysical properties reported herein.

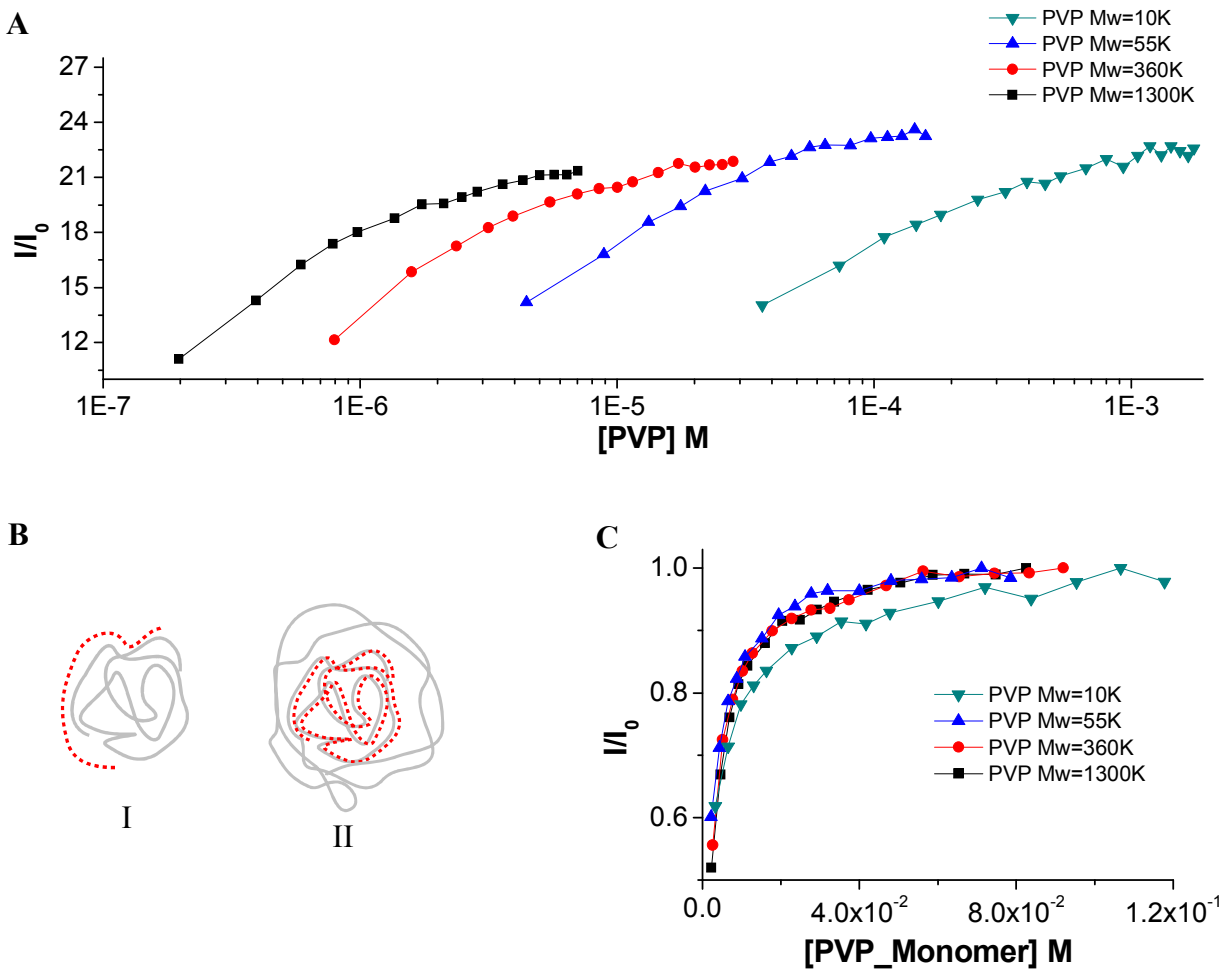

Figure 3: (A) Fluorescence enhancement versus the amphiphilic polymer concentration upon incremental addition of 10K, 55K, 360K and 1300K of PVP to an MPS-PPV solution ($1.6x10^{-4}$M reported in monomer concentration). (B) Schematic representation of the two proposed interaction models between MPS-PPV and PVP. (C) Fluorescence enhancement acquired in (A)

plotted against PVP monomer concentration. All measurements were done in 10 mM HEPES buffer pH=7.3 and 150 mM NaCl and emission spectra were acquired upon excitation at 450nm. The lines connecting the experimental points are for visual aid.

To further elucidate the mode of interaction between the two polymers, we performed a series of quenching experiments. We chose methylviologen as it has been shown to quench by electron transfer the fluorescence emission of MPS-PPV effectively.[30] Therefore unprotected segments are prone to quenching Figure 4 summarizes the stern-volmer plots obtained for the different nanohybrid structures (PVP:MPS-PPV 150:1 monomer ratio). With the exception of PVP 10K, all particles showed an unquenchable fraction (I_0/I= 1.25) reflecting that 80% of the MPS-PPV is inaccessible to MV^{2+} and buried at the core of the amphiphilic macromolecule. This result reinforces the previous conclusion. We hypothesized that the short polymer length of PVP (10K) is unable to interact with the entire MPS-PPV backbone thus exposing an additional fraction of the conjugated polymer to the quencher. On the other hand, larger PVP molecular weights (55K, 360K and 1300K) shield efficiently the MPS-PPV backbone. As a result, the unquenchable (protected) fraction is greater with larger amphiphlic polymers. Unless otherwise stated, the PVP molecular weight that will be used in the following experiments is equal to 55K.

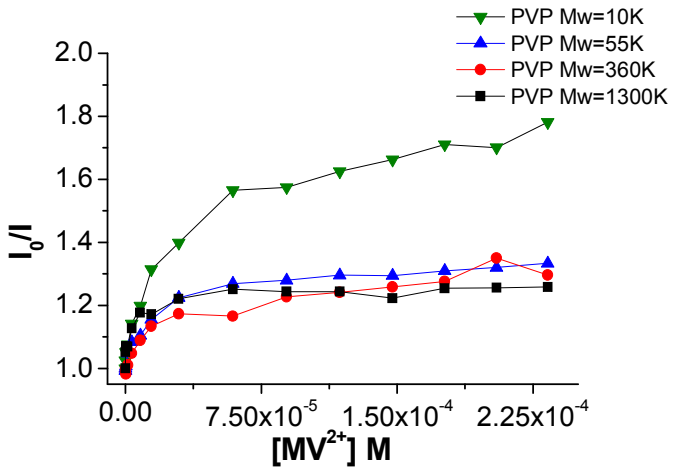

Figure 4: Stern-volmer plots for MPS−PPV/PVP nanohybrid solutions prepared with different PVP molecular weights at PVP:MPS-PPV 150:1 monomer ratio, upon adding increasing MV^{2+} concentrations. Experiments are done in 150 mM NaCl and 10 mM HEPES buffer solutions at pH=7.2. The lines connecting the experimental points are a visual aid.

Nanohybrid Photostability: We next focused our attention on evaluating the nanohybrid photostability. It was of great interest to us to prepare, in addition to a bright nanohybrid, a photostable particle that could be implemented in imaging applications and single molecule biosensing assays. Pristine conjugated polymer and nanohybrid solutions were subjected to continuous excitation at 450nm; MPS-PPV exhibited a decay over time (20% of the original intensity was lost over 10^4 seconds; Figure 5). In a marked contrast, the nanohybrid solution fluorescence intensity increased over the same time window by 18%. Nanohybrid particles prepared with different PVP molecular weights (10K and 360K in addition to 55K; SI. Fig. S.1) were tested. Both higher PVP molecular weight polymers (55K and 360K) showed similar photostability and an intensity increase of 6% within the first $4x10^3$seconds. When compared to the smallest PVP molecular weight, only a 3% increase was observed. Based on the previous quenching experiments and the image gained of the polymer-polymer interaction, we can infer that the CPE photostability is intertwined with the intimate backbone contacts of the two polymers.

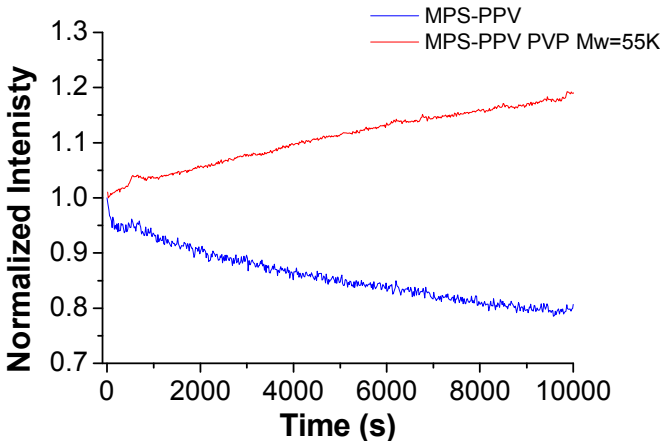

Figure 5: Intensity versus time trajectories of MPS-PPV and MPS-PPV/PVP (PVP:MPS-PPV 150:1 monomer ratio) nanohybrid upon continuous excitation at 450 nm. The experiment was done in 10 mM HEPES buffer pH=7.3 and 150 mM NaCl and emission spectra were acquired upon excitation at 450nm.

To explain why are we observing the increase in fluorescence intensity and how is PVP contributing to MPS-PPV photostability, we resorted to single particle spectroscopy experiments. We monitored individual nanohybrid fluorescence emission using a stage scanning inverted fluorescence microscope coupled to an Argon laser with continuous excitation at 488nm.

The emission was collected with a high numerical aperture objective and was directed to an avalanche photodiode detector (APD). All images showed diffraction-limited spots (*ca.* 300 nm in diameter) resulting from the emission of the nanohybrid particles (Figure 6).We then acquired intensity vs. time trajectories of single nanohybrid particles upon continuous excitation at 488 nm (Figure 7).

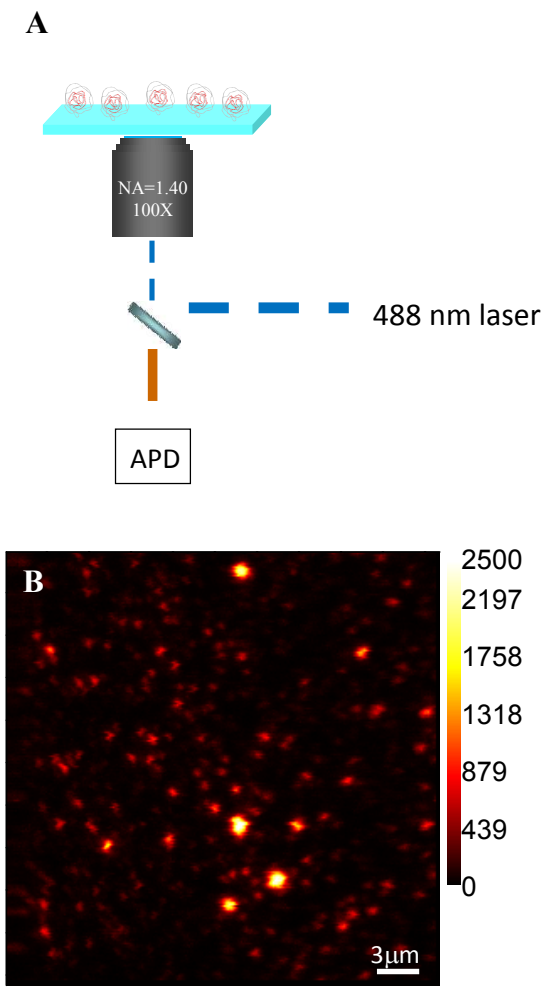

Figure 6: (A) A simplified representation of the single particle setup. (B) A 30x30 μm^2 single particle fluorescence scanning confocal image obtained upon 488 nm excitation of the nanohybrid structure prepared at PVP:MPS-PPV 150:1 monomer ratio. The right bar illustrates the counts per millisecond per pixel.

None of the recorded traces showed a sign of blinking which is highly beneficial for real-time single particle tracking. The resulting trajectories can be categorized into three distinctive patterns. 16 % showed no change in intensity and only 9% showed exponential photodegradation. The majority (75% of all recorded traces) however showed an initial increase

in the intensity followed by a steady decrease (Figure 8). On average, the intensity increased by 1.8 folds within the first 31 seconds (SI Fig S.2). After 4 minutes of continuous excitation, we observed, on average, only an 18% decrease from the original intensity. [47] Similar pattern has been previously observed by McGniel *et al.* at the ensemble level when conjugated nanodots made of poly(2,5-di(3=,7=-dimethyloctyl)phenylene-1,4-ethynylene where continuously excited.[48] The fluorescence intensity peaked at around 4 minutes before it started to decrease.

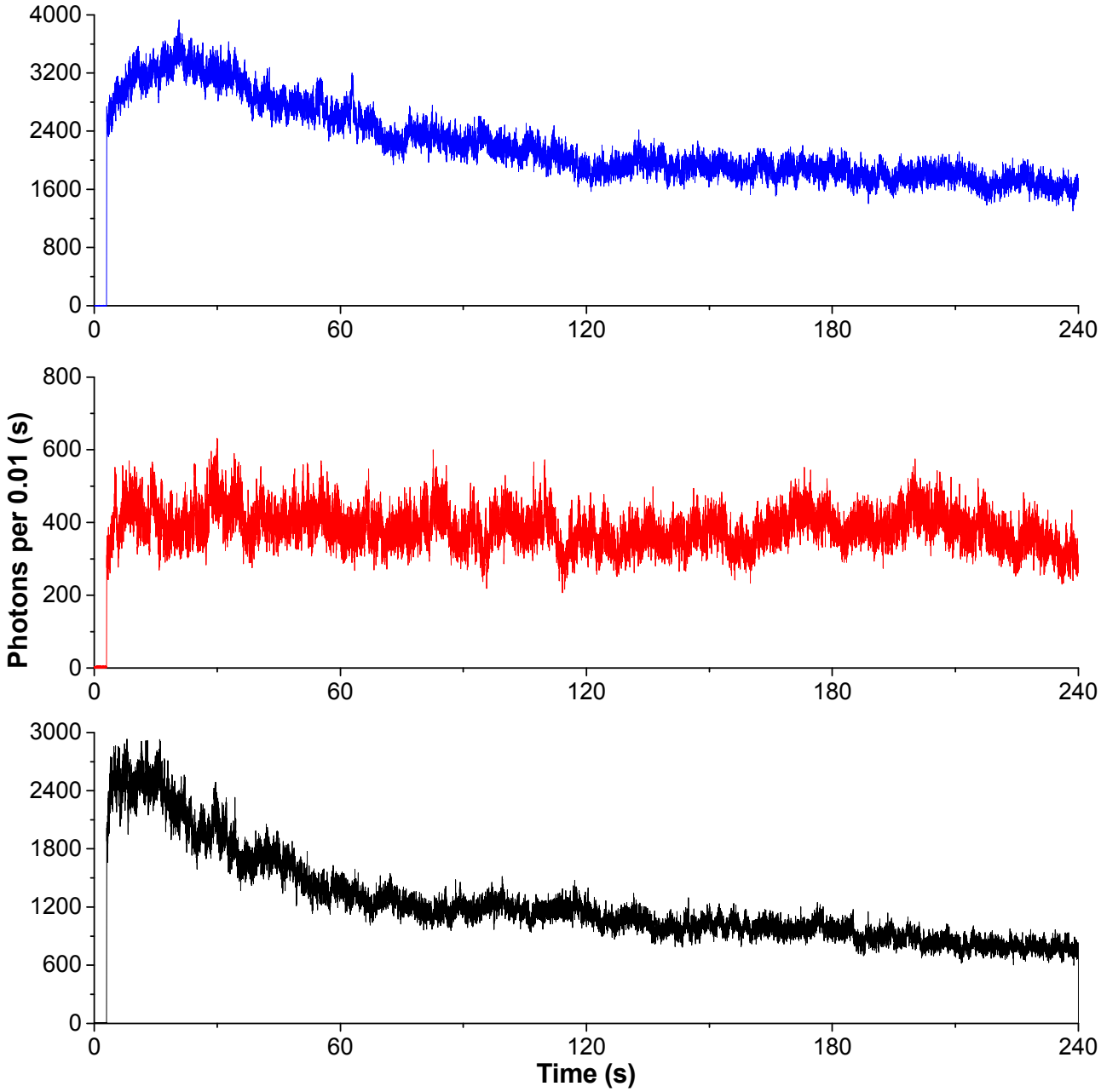

Figure 7: Intensity-time trajectories of the single particle nanohybrid acquired upon 488-nm excitation. The three traces represent the three different categories of the intensity change over time.

To explain this unique behavior, we tested few hypothesis; we first argued that this increase is due to conformation restructuring and energy minimization between the two polymers leading to

an increase in backbone extension /stabilization of the system over time. Given that the single particle traces were sequentially acquired with a time difference of few hours between some traces, the first hypothesis was quickly dropped.

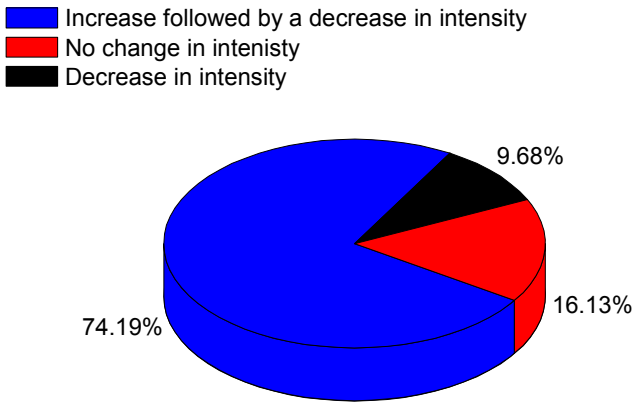

Figure 8: Statistical distribution of the intensity-time trajectories of the single particle nanohybrid.

We then considered the probability that polymer restructuring is catalyzed by the thermal energy provided by the focused excitation beam. Indeed, a nanohybrid solution showed a 16% increase in fluorescence intensity after 5 mins incubation at 35^0C (SI Fig S.3). However, based on theoretical calculations reported by Hell *et al.,* the temperature increase under our experimental conditions would not exceed 0.2-0.3K.[49] In addition, the glass coverslip onto which the nanohybrid is deposited would act as an efficient heat sink.

The inherited complex photophysics of conjugated polyelectrolytes in addition to the strong backbone-backbone interaction with PVP might hold the answer to this unusual behavior. Individual conjugated polyelectrolyte polymer, as stated earlier, could be described as a chain of multiple connected chromophores. In a highly concentrated solution of fluorophores, given the short distance between molecules, intermolecular Förster resonance energy transfer may occur leading to efficient self-quenching. Over time, and upon photodegradation, the active fluorescent molecule concentration decreases leading to an increase in the fluorescent signal. In a similar fashion, photodegradation of the highly concentrated chromophores per polymer chain reduces the number of emissive sites leading to "chromophore dilution" over time. As a result, quenching by energy transfer is dramatically reduced leading to the observed fluorescent enhancement. Upon continues irradiation, the chromophore reaches a tipping point where the enhancement by the dilution effect is overtaken by its continuous photodestruction. This eventually results in the gradual decrease in the fluorescence intensity of the single nanohybrid particle.

The amount of photons emitted, on average, per trace within our experimental window (240 s) was equal to 1.85 $x10^9$ (None of the recorded traces did completely photobleach only 18% of the original intensity was lost on average*).* This amount of emitted photons is one the highest reported so far and by far better than freely floating MPS-PPV.[26] When compared to other organic fluorophores, Cy5, for instance, would emit $6.5x10^5$ photons before irreversible photobleaching and Alexa 633 around $9.3x10^6$.[50] Conjugated polymer dots prepared from conjugated polymers were reported to emit between 10^6 and 10^9 before complete irreversible photobleaching. [48, 51]

CPE photostability in general is attributed to the protection from molecular oxygen provided by surfactants.[38] However, in our specific case, PVP macromolecules are known to be oxygen

permeable.[52, 53] In a recent single molecule study, Scheblykin *et al.* showed that the collision between freely diffusing conjugated polymers lead to the simultaneous rupture of polymer chains.[54] The mechanical bending of the stiff conjugated macromolecules upon impact can weaken the chemical bond and markedly catalyze the photochemical oxygen reaction at the contact point. This in turn accelerates chain degradation by at least 20 times. In addition, chain bending was found to be also accentuated by prolonged polymer backbone interaction. Based on the previously discussed molecular interaction, we believe that the intimate backbone interactions between PVP and the anionic conjugated polyelectrolyte is providing a protective shell against interchain impact and inhibiting prolonged backbone interactions thus increasing the photostability of the conjugated polyelectrolyte. It also explains why the short PVP (10K) did not protect, as efficiently, the CPE from photodegradation.

Tuning the fluorescent intensity of the nanohybrid particles: Based on all the previous results and the acquired molecular understanding of the interaction between MPS-PPV and PVP, we speculated that the intensity of the nanohybrid particles could be tuned by modifying the order of addition (Figure 9). When MPS-PPV is added to a solution of PVP, the amphiphilc macromolecules will compete to complex with the newly added MPS-PPV resulting in a homogenous distribution of CPEs among the nanohybrid particles (Sample 1). However, When PVP is added to a solution of MPS-PPV, the first amphiphilic macromolecules will be exposed to a large amount of anionic CPEs. Consequently, each PVP polymer will scavenge multiple CPEs (Sample 2). To verify our hypothesis, we examined the two samples at the single particle level.

As described earlier, single particle confocal images were acquired. Fluorescence intensities were calculated for each particle and their distributions are summarized in Figure 9B. When PVP

is added to MPS-PPV, the average photon count per particle was equal to 683 with a standard deviation of 147. The other order of addition yielded an average of photon count per particle of 275 with a standard deviation of 91. As expected, the addition of PVP to a solution of MPS-PPV (rather than the addition of MPS-PPV to PVP) generates brighter MPS-PPV/PVP hybrids. This result offers a simple way to tune the nanohybrid particle intensity.

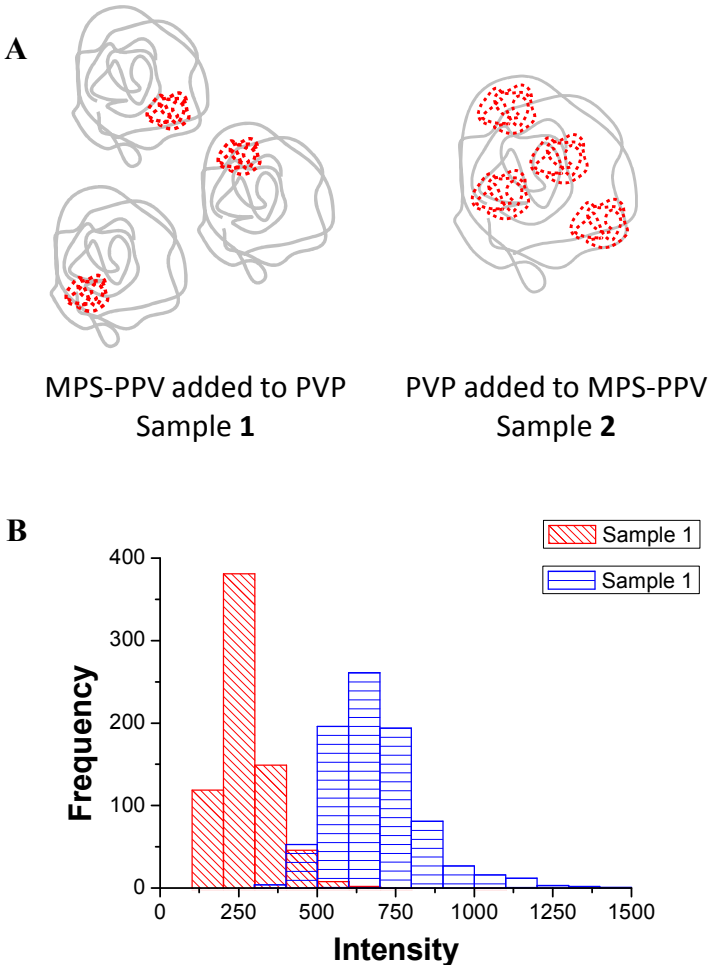

Figure 9: (A) Schematic illustration of a potential interaction of MPS-PPV in complex with PVP based on the order of addition. (B) Intensity distribution histograms extracted from single particle confocal images of sample 1 and sample 2.

Conclusion: We report herein a straightforward method to prepare photostable, bright and none blinking nanohybrid particles by complexing an anionic conjugated polyelectrolytes with PVP. By employing ensemble and single particle spectroscopy methods, we unraveled the mode of interaction between the two polymers, quantified the amount of photon emitted per particle and explained the mechanism behind its photostability. The fluorescence intensity can be easily tuned by simply changing the order of addition. It is therefore possible to tune the particle brightness by using different PVP molecular weights. Given the unique and improved photostability, the nanohybrid particles can prove instrumental in current state-of-the-art single molecule tracking, bioimaging and single molecule/particle based sensing assays.

Methods:

Chemicals: poly[5-methoxy-2-(3-sulfopropoxy)-1,4-phenylenevinylene]potassiumsalt(MPS-PPV), HEPES sodium salt, polyvinylpyrrolidone(Average Mw 10K; 55K; 360K; 1,300K), Methyl viologen dichloride hydrate 98% were purchased from Sigma-Aldrich.

Absorption and Emission Spectrum: Steady-state fluorescence spectroscopy was carried out using a Thermo Scientific Lumina spectrophotometer. Absorption spectra were recorded using a Jasco V-570 UV−vis spectrophotometer in double-beam mode. For all steady-state absorption and emission experiments, the solutions were placed in 1 cm × 1 cm quartz cuvettes.

Quenching Experiments: Concentrated solutions of methyl viologen were prepared on the same day of the quenching experiment. Aliquots of methyl viologen in 150 mM NaCl, 10 mM

HEPES, pH 7.2-7.4 were added to the samples, and fluorescence spectra were taken immediately after mixing.

Single Molecule Experiments: Sample preparation: glass coverslips were cleaned in a piranha solution (15: 5 mL H_2SO_4:H_2O_2) for 1 hour. Flow chambers were prepared with a predrilled polycarbonate film (GraceBio) with an adhesive gasket which was assembled on top of the cleaned surface yielding a chamber with a total volume of 10 μL. Nano-hybrid particles in the concentratin range of 10^{-9} M were injected into the chanber. All experiments were run under a constant flow of an oxygen scavenger solution consisting of β-mercaptoethanol 1% v/v, β-D(+)glucose 3% w/v, glucose oxidase 0.1 mg/mL, and catalase 0.02 mg/mL. Solutions were 10 mM in HEPES buffer pH 7.3 and 150 mM in NaCl. All experiments were conducted at room temperature (22-23 °C).

Confocal Imaging: The experimental setup consisted of an Olympus IX-71 inverted microscope operated in a confocal form and provided with a closed-loop sample scanning stage (Nano LP100, Mad City Labs, Madison, WI) used for imaging and sample positioning. Samples were excited continuously employing the 488 nm (53 $W.cm^{-2}$) from output from an Ar+ laser. The circularly polarized laser beam was introduced via a single mode fiber optic and directed by a dichroic beamsplitter (z488rdc DCLP, Chroma, Rockingham, VT) to the sample via a high numerical aperture (NA = 1.40) oil immersion objective (Olympus U PLAN SAPO 100X). Fluorescence emission was collected through the same objective and then directed to an avalanche photodiode detector (PerkinElmer Optoelectronics SPCM-AQR-14, Vaudreuil, Quebec, Canada). The emission was cleaned from any residual laser excitation by an HQ500LP (from Chroma, Rockingham, VT). Images consisting of 256 by 256 pixels were acquired by collecting the intensity for 1 ms at each pixel. Intensity-time trajectories were recorded at 1 ms

dwell time by positioning the stage on a single nanohybrid particle. A home built LabView routine was used for data acquisition and stage positioning. A National Instruments NI-PCI-6602 board was used as a counter board.

Supplementary Information. Dynamic light scattering, Photostability of different nanohybrids, and emission and absorption spectrum are available in the supporting information.

AUTHOR INFORMATION

Corresponding Author

*To whom correspondence should be addressed:
Phone: 961-1-350000 Ext 3989 **Fax:** 961-1-350000 Ext 3970 **Email:** pk03@aub.edu.lb

Funding Sources

TWAS (Award number: 12-316 RG/MSN/AF/AC_C; UNESCO FR 3240270863) and the University research board (Award number: 102848)

ACKNOWLEDGMENT

The authors are grateful to Dr. Gonzalo Cosa's Laboratory at McGill University for providing access to their single molecule spectroscopy setup. This work was supported by TWAS (Award number: 12-316 RG/MSN/AF/AC_C; UNESCO FR 3240270863) and the University research board (Award number: 102848)

REFERENCES

1. A. T. Ngo, P. Karam and G. Cosa, *Pure and Applied Chemistry*, 2010, **83**, 43-55.
2. H. Jiang, P. Taranekar, J. R. Reynolds and K. S. Schanze, *Angewandte Chemie International Edition*, 2009, **48**, 4300-4316.
3. J. H. Seo, A. Gutacker, Y. Sun, H. Wu, F. Huang, Y. Cao, U. Scherf, A. J. Heeger and G. C. Bazan, *Journal of the American Chemical Society*, 2011, **133**, 8416-8419.
4. Z. He, C. Zhong, S. Su, M. Xu, H. Wu and Y. Cao, *Nature Photonics*, 2012, **6**, 591-595.
5. Z. He, C. Zhong, X. Huang, W. Y. Wong, H. Wu, L. Chen, S. Su and Y. Cao, *Advanced Materials*, 2011, **23**, 4636-4643.

6. L. Lu, F. H. Rininsland, S. K. Wittenburg, K. E. Achyuthan, D. W. McBranch and D. G. Whitten, *Langmuir*, 2005, **21**, 10154-10159.
7. P. Karam, A. A. Hariri, C. F. Calver, X. Zhao, K. S. Schanze and G. Cosa, *Langmuir*, 2014, **30**, 10704-10711.
8. K. Ogawa, S. Chemburu, G. P. Lopez, D. G. Whitten and K. S. Schanze, *Langmuir*, 2007, **23**, 4541-4548.
9. S. Chemburu, E. Ji, Y. Casana, Y. Wu, T. Buranda, K. S. Schanze, G. P. Lopez and D. G. Whitten, *The Journal of Physical Chemistry B*, 2008, **112**, 14492-14499.
10. K. Achyuthan, T. Bergstedt, L. Chen, R. Jones, S. Kumaraswamy, S. Kushon, K. Ley, L. Lu, D. McBranch and H. Mukundan, *Journal of Materials Chemistry*, 2005, **15**, 2648-2656.
11. D. Wang, X. Gong, P. S. Heeger, F. Rininsland, G. C. Bazan and A. J. Heeger, *Proceedings of the National Academy of Sciences*, 2002, **99**, 49-53.
12. J. Liang, K. Li and B. Liu, *Chemical Science*, 2013, **4**, 1377-1394.
13. M. R. Pinto and K. S. Schanze, *Proceedings of the National Academy of Sciences of the United States of America*, 2004, **101**, 7505-7510.
14. C. Tan, M. R. Pinto and K. S. Schanze, *Chemical Communications*, 2002, 446-447.
15. S. W. Thomas, G. D. Joly and T. M. Swager, *Chemical Reviews*, 2007, **107**, 1339-1386.
16. Q. Zhou and T. M. Swager, *Journal of the American Chemical Society*, 1995, **117**, 7017-7018.
17. B. S. Gaylord, A. J. Heeger and G. C. Bazan, *Proceedings of the National Academy of Sciences*, 2002, **99**, 10954-10957.
18. B. S. Gaylord, A. J. Heeger and G. C. Bazan, *Journal of the American Chemical Society*, 2003, **125**, 896-900.
19. B. Liu and G. C. Bazan, *Chemistry of materials*, 2004, **16**, 4467-4476.
20. X. Zhao, Y. Liu and K. S. Schanze, *Chemical Communications*, 2007, 2914-2916.
21. L. Chen, D. W. McBranch, H.-L. Wang, R. Helgeson, F. Wudl and D. G. Whitten, *Proceedings of the National Academy of Sciences*, 1999, **96**, 12287-12292.
22. A. Duarte, A. Chworos, S. F. Flagan, G. Hanrahan and G. C. Bazan, *Journal of the American Chemical Society*, 2010, **132**, 12562-12564.
23. P. A. Dalgarno, C. A. Traina, J. C. Penedo, G. C. Bazan and I. D. W. Samuel, *Journal of the American Chemical Society*, 2013, **135**, 7187-7193.
24. K.-Y. Pu and B. Liu, *Advanced Functional Materials*, 2011, **21**, 3408-3423.
25. T. Huser, M. Yan and L. J. Rothberg, *Proceedings of the National Academy of Sciences*, 2000, **97**, 11187-11191.
26. P. Karam, A. T. Ngo, I. Rouiller and G. Cosa, *Proceedings of the National Academy of Sciences*, 2010, DOI: 10.1073/pnas.1008068107.
27. M. Yan, L. Rothberg, F. Papadimitrakopoulos, M. Galvin and T. Miller, *Physical review letters*, 1994, **73**, 744.
28. .
29. G. A. Montano, A. M. Dattelbaum, H.-L. Wang and A. P. Shreve, *Chemical Communications*, 2004, DOI: 10.1039/b401682c, 2490-2491.
30. A. T. Ngo and G. Cosa, *Langmuir*, 2009, **26**, 6746-6754.
31. A. T. Ngo, P. Karam, E. Fuller, M. Burger and G. Cosa, *Journal of the American Chemical Society*, 2008, **130**, 457-459.
32. Y. Liu, K. Ogawa and K. S. Schanze, *Analytical Chemistry*, 2007, **80**, 150-158.

33. M. L.-Viger, D. Brouard and D. Boudreau, *The Journal of Physical Chemistry C*, 2011, **115**, 2974-2981.
34. S. H. Lee, S. Kömürlü, X. Zhao, H. Jiang, G. Moriena, V. D. Kleiman and K. S. Schanze, *Macromolecules*, 2011, **44**, 4742-4751.
35. D.-L. Jiang, C.-K. Choi, K. Honda, W.-S. Li, T. Yuzawa and T. Aida, *Journal of the American Chemical Society*, 2004, **126**, 12084-12089.
36. J.-M. Koenen, X. Zhu, Z. Pan, F. Feng, J. Yang and K. S. Schanze, *ACS Macro Letters*, 2014, **3**, 405-409.
37. R. D. Scurlock, B. Wang, P. R. Ogilby, J. R. Sheats and R. L. Clough, *Journal of the American Chemical Society*, 1995, **117**, 10194-10202.
38. W. Dou, C. Wang, G. Wang, Q. Ma and X. Su, *The Journal of Physical Chemistry B*, 2008, **112**, 12681-12685.
39. H.-W. Liu, A. T. Ngo and G. Cosa, *Journal of the American Chemical Society*, 2011, **134**, 1648-1652.
40. V. P. Torchilin, T. S. Levchenko, K. R. Whiteman, A. A. Yaroslavov, A. M. Tsatsakis, A. K. Rizos, E. V. Michailova and M. I. Shtilman, *Biomaterials*, 2001, **22**, 3035-3044.
41. J. Huang, L. H. Bu, J. Xie, K. Chen, Z. Cheng, X. G. Li and X. Y. Chen, *ACS Nano*, 2010, **4**, 7151-7160.
42. H. Y. Lee, A. Y. Seol, K. H. Jeong and Y. J. Kim, *Macromolecular Research*, 2007, **15**, 547-552.
43. H. Kamada, Y. Tsutsumi, Y. Yamamoto, T. Kihira, Y. Kaneda, Y. Mu, H. Kodaira, S.-i. Tsunoda, S. Nakagawa and T. Mayumi, *Cancer research*, 2000, **60**, 6416-6420.
44. U. Resch-Genger, M. Grabolle, S. Cavaliere-Jaricot, R. Nitschke and T. Nann, *Nature methods*, 2008, **5**, 763-775.
45. S. Tretiak, A. Saxena, R. Martin and A. Bishop, *Physical review letters*, 2002, **89**, 097402.
46. R. Godin, R. E. Palacios and G. Cosa, *The Journal of Physical Chemistry C*, 2015, **119**, 12875-12886.
47. .
48. C. Wu, B. Bull, C. Szymanski, K. Christensen and J. McNeill, *ACS Nano*, 2008, **2**, 2415-2423.
49. A. Schönle and S. W. Hell, *Opt. Lett.*, 1998, **23**, 325-327.
50. T. Schmidt, U. Kubitscheck, D. Rohler and U. Nienhaus, *Single Molecules*, 2002, **3**, 327-327.
51. C. Wu, C. Szymanski, Z. Cain and J. McNeill, *Journal of the American Chemical Society*, 2007, **129**, 12904-12905.
52. J. Wichterlová, K. Wichterle and J. Michálek, *Polymer*, 2005, **46**, 9974-9986.
53. J. Hadassah and P. K. Sehgal, *Clinical and Experimental Optometry*, 2006, **89**, 374-380.
54. Y. Tian, M. V. Kuzimenkova, M. Xie, M. Meyer, P.-O. Larsson and I. G. Scheblykin, *NPG Asia Mater*, 2014, **6**, e134.